RIA Superconducting Drift Tube Linac R & D: Final Report DE-FG02-06ER41412 Amendment A000

J. Popielarski, J. Bierwagen, S. Bricker, C. Compton, J. DeLauter, P. Glennon, T. Grimm*, W. Hartung, D. Harvell, M. Hodek, M. Johnson, F. Marti, P. Miller, A. Moblo, D. Norton, L. Popielarski, J. Wlodarczak, R. C. York, A. Zeller
National Superconducting Cyclotron Laboratory, Michigan State University, East Lansing, Michigan

21 May 2009

Abstract

Cavity and cryomodule development work for a superconducting ion linac has been underway for several years at the National Superconducting Cyclotron Laboratory. The original application of the work was the proposed Rare Isotope Accelerator. At present, the work is being continued for use with the Facility for Rare Isotope Beams (FRIB). The baseline linac for FRIB requires 4 types of superconducting cavities to cover the velocity range needed to accelerate an ion beam to $\geq$ 200 MeV/u: 2 types of quarter-wave resonator (QWR) and 2 types of half-wave resonator (HWR). Superconducting solenoids are used for focussing. Active and passive shielding is required to ensure that the solenoids' field does not degrade the cavity performance. First prototypes of both QWR types and one HWR type have been fabricated and tested. A prototype solenoid has been procured and tested. A test cryomodule has been fabricated and tested. The test cryomodule contains one QWR, one HWR, one solenoid, and one super-ferric quadrupole. This report covers the design, fabrication, and testing of this cryomodule.

*Present address: Niowave, Inc., 1012 North Walnut St, Lansing, Michigan 48906 USA

Contents

1 Introduction 3

2 Half-Wave Resonator 3
- 2.1 Design and Fabrication . . . 4
- 2.2 Experimental Results . . . 6

3 Quarter-Wave Resonator 8
- 3.1 Design and Fabrication . . . 8
- 3.2 Experimental Results . . . 8

4 Magnets 13

5 Magnetic Shielding 13

6 Shielding Tests 14

7 Cryomodule Design 14
- 7.1 RF Couplers . . . 18
- 7.2 Tuners . . . 18
- 7.3 Cold Box . . . 19

8 Cryomodule Fabrication 21

9 Cryomodule Testing 21
- 9.1 Cool-Down . . . 22
- 9.2 Static Heat Leak . . . 22
- 9.3 RF Testing of QWR . . . 22
- 9.4 RF Testing of HWR . . . 24
- 9.5 X-Ray Spectrum Measurements . . . 27
- 9.6 Solenoid Operation . . . 31
- 9.7 RF Couplers . . . 31
- 9.8 Tuners . . . 31
- 9.9 Frequency Issues . . . 31

10 Conclusion 33

11 Acknowledgments 34

1 Introduction

The development work described in this report was done as part of the research and development program for the proposed Rare Isotope Accelerator (RIA). The RIA main accelerator was conceived as a linac for heavy and light ions, which would to accelerate the ions to 400 MeV per nucleon with a beam power up to 400 kW [1]. This required a 1400 MV superconducting linac. A design based on 80.5 MHz was developed by the National Superconducting Cyclotron Laboratory (NSCL) at Michigan State University (MSU).

A less energetic linac is presently being planned as part of the Facility for Rare Isotope Beams (FRIB). FRIB includes a 200 MeV per nucleon linac for ions with a beam power of up to 400 kW. FRIB includes an option for a later energy upgrade to 400 MeV per nucleon. Because of the similarities between the original RIA linac concept and the present-day FRIB linac design, the development work described herein will be directly applicable to FRIB.

A rectangular cryomodule design with a cryogenic alignment rail was developed for the linac. The same basic design can be used for all of the superconducting cavity and magnet types needed for the linac. A prototype 2-cavity cryomodule for $\beta = v/c = 0.47$ elliptical cavities was designed in 2003 [2] and tested in 2004 [3]. This cryomodule design is suitable for the FRIB upgrade, which would require elliptical cavities with $\beta = 0.61$ and $\beta = 0.81$. A similar cryomodule design has been developed for the lower-β quarter wave resonators (QWRs) and half-wave resonators (HWRs), which are interspersed with superconducting magnets for focussing.

A second prototype cryomodule was designed and fabricated for testing of lower-β cavities and focussing elements as a unit. The test cryomodule contains one $\beta = 0.085$ QWR [4], one $\beta = 0.285$ HWR [5], one superconducting solenoid with a dipole steering coil, and one super-ferric quadrupole [6]. The QWR and HWR are both "first generation" prototypes without any stiffening elements. A Ti rail system is used for support and alignment. Active and passive magnetic shielding is implemented, consisting of reverse wound coils at the ends of the solenoid, a Meissner shield (Nb can) around the solenoid, and μ metal shields around the Meissner shield and the cavities. Additional information about the low-β prototype cryomodule design can be found in a separate paper [7]. Some preliminary results of the cryomodule test have also been reported previously [8].

This report covers the cavity design, fabrication, and testing; magnet and magnetic shielding design, fabrication, and testing; design and fabrication of auxiliary cryomodule components; and cryomodule design, fabrication, and testing.

2 Half-Wave Resonator

The $\beta = 0.285$ half-wave resonator (HWR) was fabricated and tested in a Dewar [5] prior to installation in the test cryomodule. Most of the fabrication work for the HWR was done at NSCL. The electron beam welding was done with industry.

2.1 Design and Fabrication

Drawings of the HWR are shown in Figure 1. The cavity was fabricated from niobium of RRR ≥ 150. The inner conductor (100 mm inner diameter) and outer conductor (240 mm inner diameter) were formed from 2 mm Nb sheet. Both tubes were rolled, welded, and pressed into their final shape. The upper and lower shorting plates were machined from 19 mm Nb plate. The remaining parts were machined from Nb rod. Probe antennae (coupling to the electric field) were used for both the input coupler and the pick-up, so that the RF ports could be placed at the median plane of the cavity. For simplicity, the RF ports were identical to the beam ports (reactor grade Nb was used for all 4 ports; the inner diameter was 30 mm). These 4 ports were the only access to the cavity for chemical etching and high-pressure rinsing. For expedience, indium was used for vacuum seals, and initial testing was done without a helium vessel.

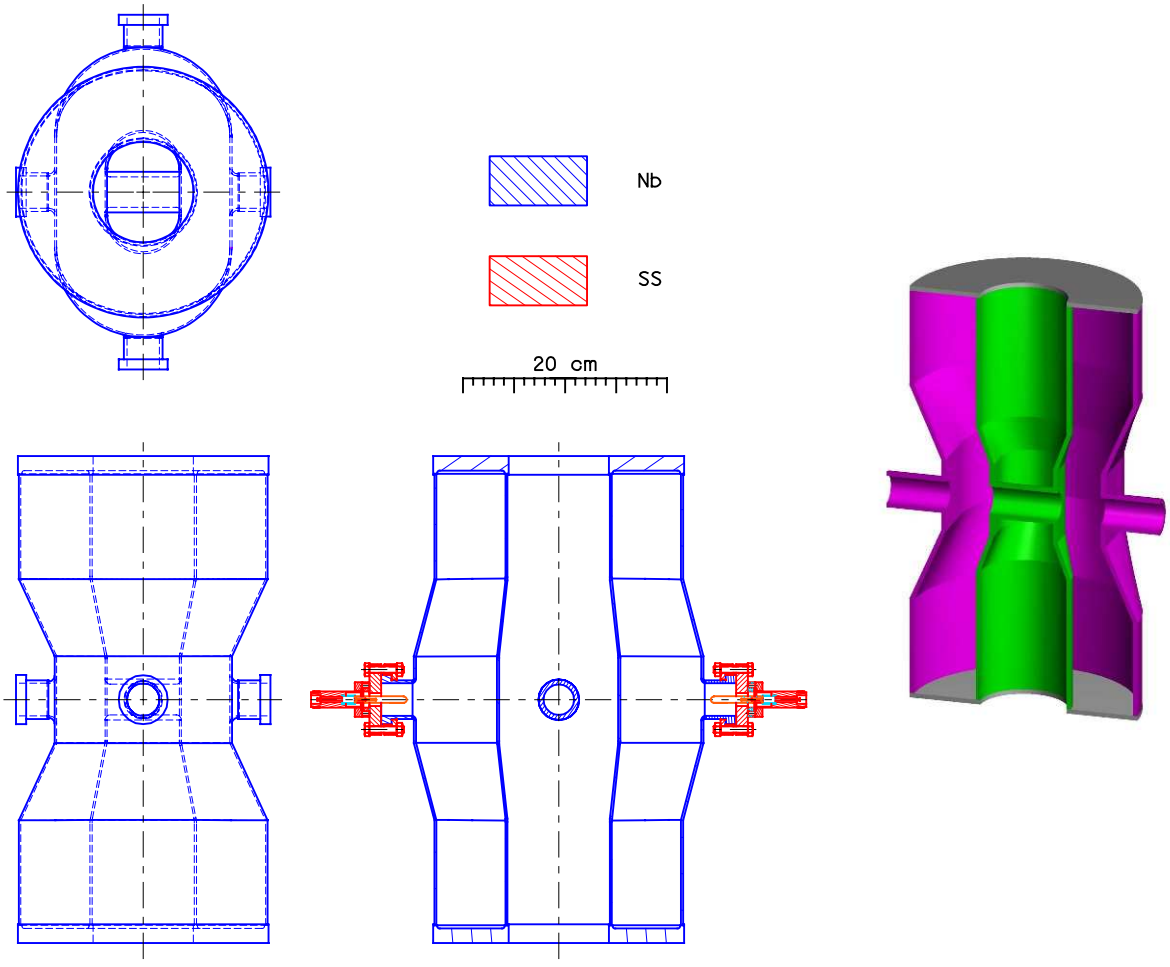

Figure 1. Drawings of the $\beta = 0.285$ HWR. Left: Three-view drawing. Right: Isometric sectional view. The side view shows the RF coupling antennae and feed-throughs.

Electron beam welding with pressure $\leq 3 \cdot 10^{-5}$ torr was used to join the niobium parts. All parts were etched > 10 μm prior to welding. Figure 2a shows the niobium parts before final welding. Figure 2b shows the inside of the partially assembled cavity.

After welding, the completed HWR was etched with a Buffered Chemical Polishing (BCP) solution (1:1:2 mixture by volume of concentrated hydrofluoric, nitric, and phosphoric acid) to remove 120 μm from the inside surface. The acid was circulated through a chiller in a closed loop system to maintain a temperature ≤ 15°C. After etching, a high-pressure rinse with ultra-pure water was done in a Class 100 clean room for 1 hour. The cavity was allowed to dry in the clean room. Then the vacuum ports and antennae were attached and the cavity was installed on an insert for RF testing in a vertical cryostat (Figure 2c).

Figure 2. (a) Niobium parts before final welding of HWR prototype; (b) inside view of the cavity before assembly of upper plate; (c) assembly of the cavity onto the insert for cryogenic testing.

2.2 Experimental Results

The electric field profile along the beam axis was measured via a bead pull, as shown in Figure 3. The field unflatness parameter ($\Delta E/E$) was relatively small at 2.5%.

The first RF test was done in December 2002. In the first test, the coupling strengths (Q_{ext}) were $1.4 \cdot 10^9$ and $1.6 \cdot 10^{11}$ for the input coupler and pick-up, respectively. The base pressure in the cavity at room temperature was $1.6 \cdot 10^{-8}$ torr prior to the cool-down. No vacuum bake-out was done. Upon cooling down to 4.3 K, multipacting barriers were encountered at low field (E_p = peak surface electric field = 0.25 to 0.45 MV/m). We were able to punch through the multipacting barriers after about 80 minutes of conditioning. The multipacting field levels were consistent with simulations, which predicted one-point

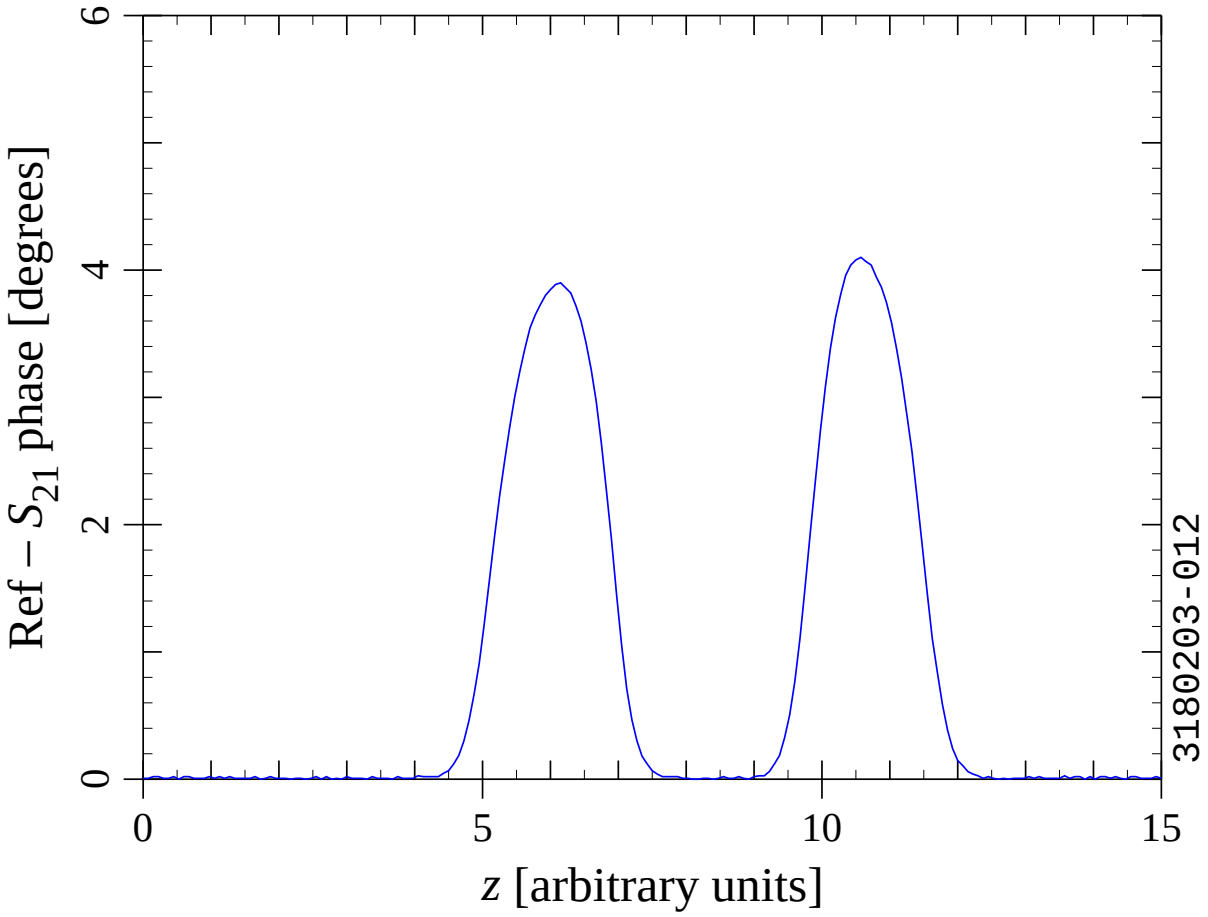

Figure 3. Bead pull measurement showing the electric field profile along the beam axis for the HWR prototype.

multipacting on the outer conductor in the high electric field region.

The measured quality factor (Q_0) as a function of field level is shown in Figure 4 for various temperatures. The FRIB design goal is $E_p = 30$ MV/m with $Q_0 \geq 8 \cdot 10^9$ at $T = 2$ K. As can be seen in Figure 4, the prototype meets the design goal.

In March 2003, the cavity was retested with a higher input Q_{ext} of $5 \cdot 10^9$. Similar peak fields were obtained, and a residual surface resistance of 5 nΩ was confirmed.

After initial Dewar testing, a helium vessel, made of titanium, was constructed around the cavity. Additional Dewar testing was done with the helium vessel and with the cavity in proximity to a magnet (see section 6).

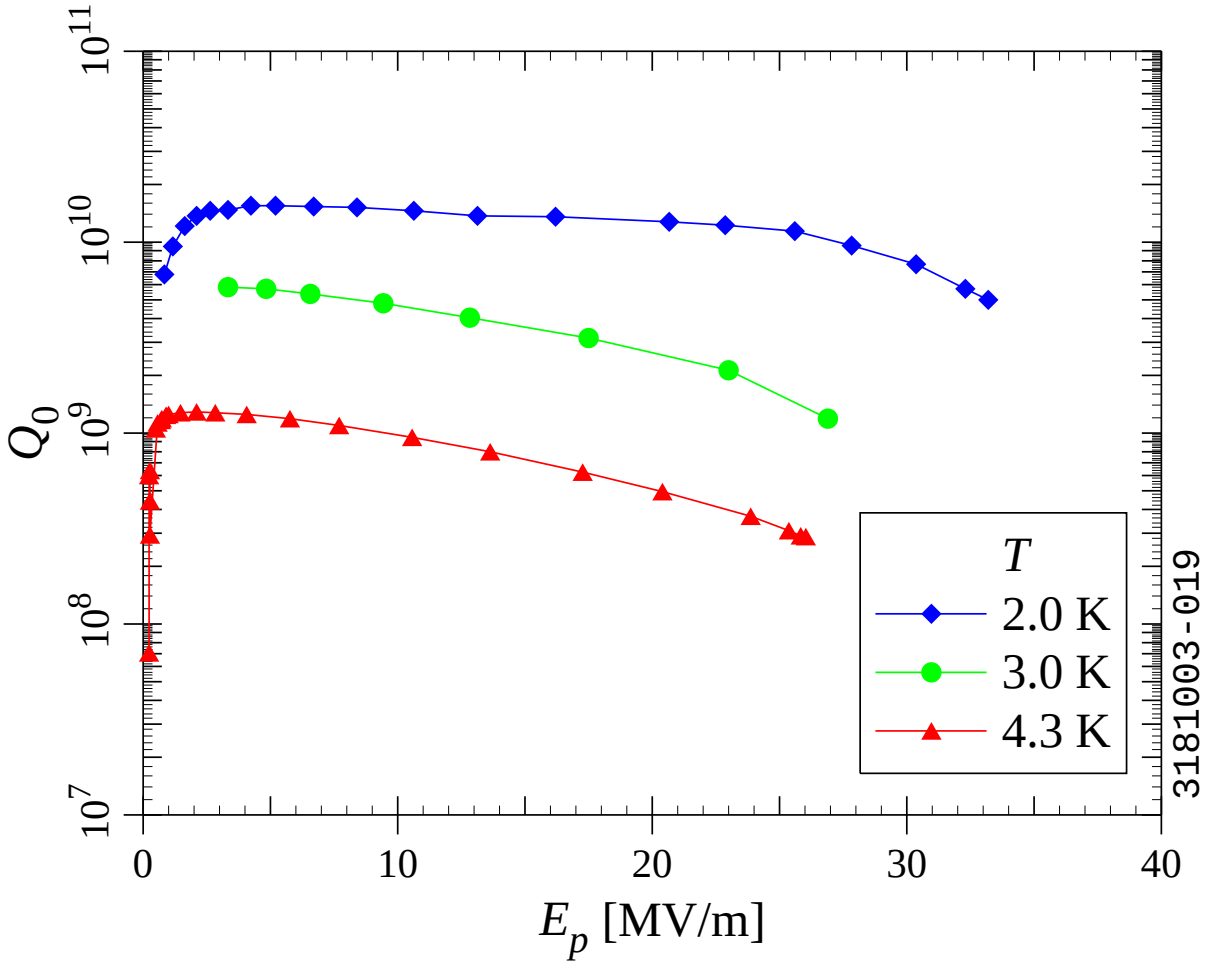

Figure 4. RF test results for the HWR prototype at various temperatures.

3 Quarter-Wave Resonator

The development of the $\beta = 0.085$ quarter-wave resonator (QWR) was undertaken as a collaboration between INFN-Legnaro and MSU [4]. The QWRs at 80 MHz presently being used at Legnaro for the ALPI and PIAVE linacs [9] provided the basis for the design.

3.1 Design and Fabrication

The ALPI and PIAVE cavities have an outer conductor diameter of 180 mm; this was enlarged to 240 mm for the $\beta = 0.085$ cavity. A larger aperture (30 mm) was also used. Another new feature is to separate the cavity vacuum from the insulation vacuum to reduce particulate contamination of the cavity surfaces. Probe couplers are used instead of loop couplers. A drawing of the structure is shown in Figure 5.

Sheet Nb of thickness 2 mm was used for the outer conductor and center conductor. The top plate, the beam tubes, and the tip of the center conductor were machined from solid Nb. Holes were machined into the latter (see Figure 5) to improve the contact with the liquid helium. The bottom flange consists of a Nb-Ti ring welded to the Nb outer conductor, mating with a stainless steel (SS) blank-off flange; a Nb tuning plate is bolted to the outer conductor via this flange. Forming of the Nb parts was done at MSU and in the local area. Electron beam welding was done by industry. High purity material (RRR ≥ 150) was used for all Nb parts except the beam tubes, which were made from reactor grade Nb rod. Figure 6a shows the Nb parts before welding, and Figure 6b shows the inside of the cavity after welding. Indium joints were used to provide a vacuum seal on the bottom flange and beam tube flanges. Electrical contact between the tuning plate and the outer conductor was made via pressure from the bottom flange (thus the indium provides a vacuum seal, but not an RF seal). At $E_p = 20$ MV/m, the magnetic field at the joint is about 0.5 mT. A small ridge was machined into the Nb plate for better RF contact with the outer conductor. A hollow tube was also installed on the bottom flange to touch the center of the tuning plate for improved heat sinking to the helium bath.

3.2 Experimental Results

After the final welding, bead pulls were done to check the field flatness. Figure 7 shows the bead pull traces. The field unflatness parameter ($\Delta E/E$) was 3.8%.

The completed QWR was etched with chilled 1:1:2 BCP to remove 120 μm from the inside surface, following the same procedures as for the HWR. After etching, a high-pressure rinse with ultra-pure water was done in a Class 100 clean room for 60 to 120 minutes. The cavity was then assembled onto an insert for RF testing. Figure 6c shows the $\beta = 0.085$ cavity just prior to insertion into the Dewar.

RF testing was done with the cavity immersed in a liquid helium bath at 4.2 K; additional measurements were done at 2 K. A phase feedback loop was used to lock onto the resonance. The RF power was provided by a 50 W amplifier protected by a circulator. Copper probe antennae (mounted on the bottom flange, see Figure 5) were used to couple the power into

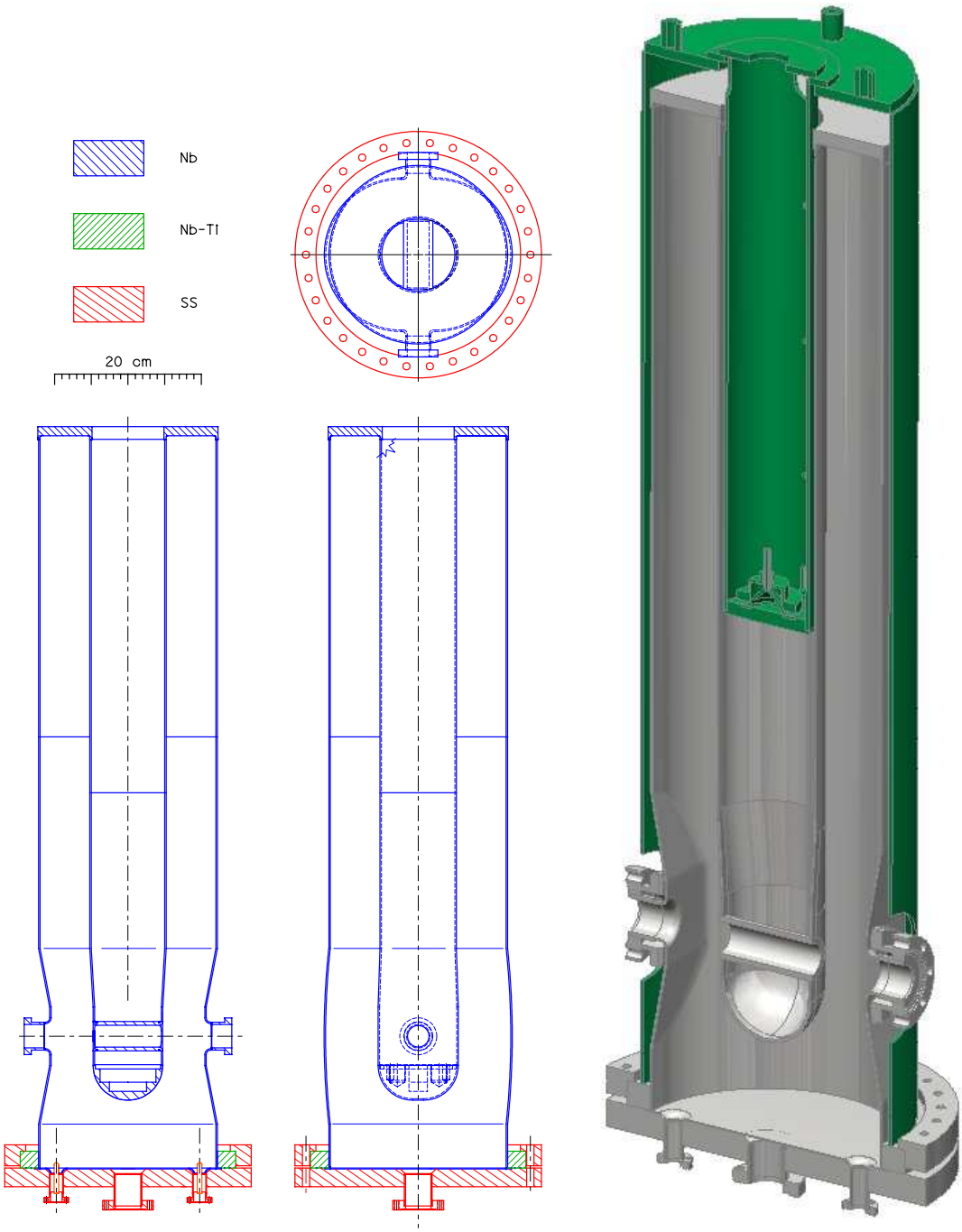

Figure 5. Drawings of the $\beta = 0.085$ QWR. Left: Three-view drawing of the cavity. Right: Isometric sectional view of the cavity after installation of the damper and helium vessel.

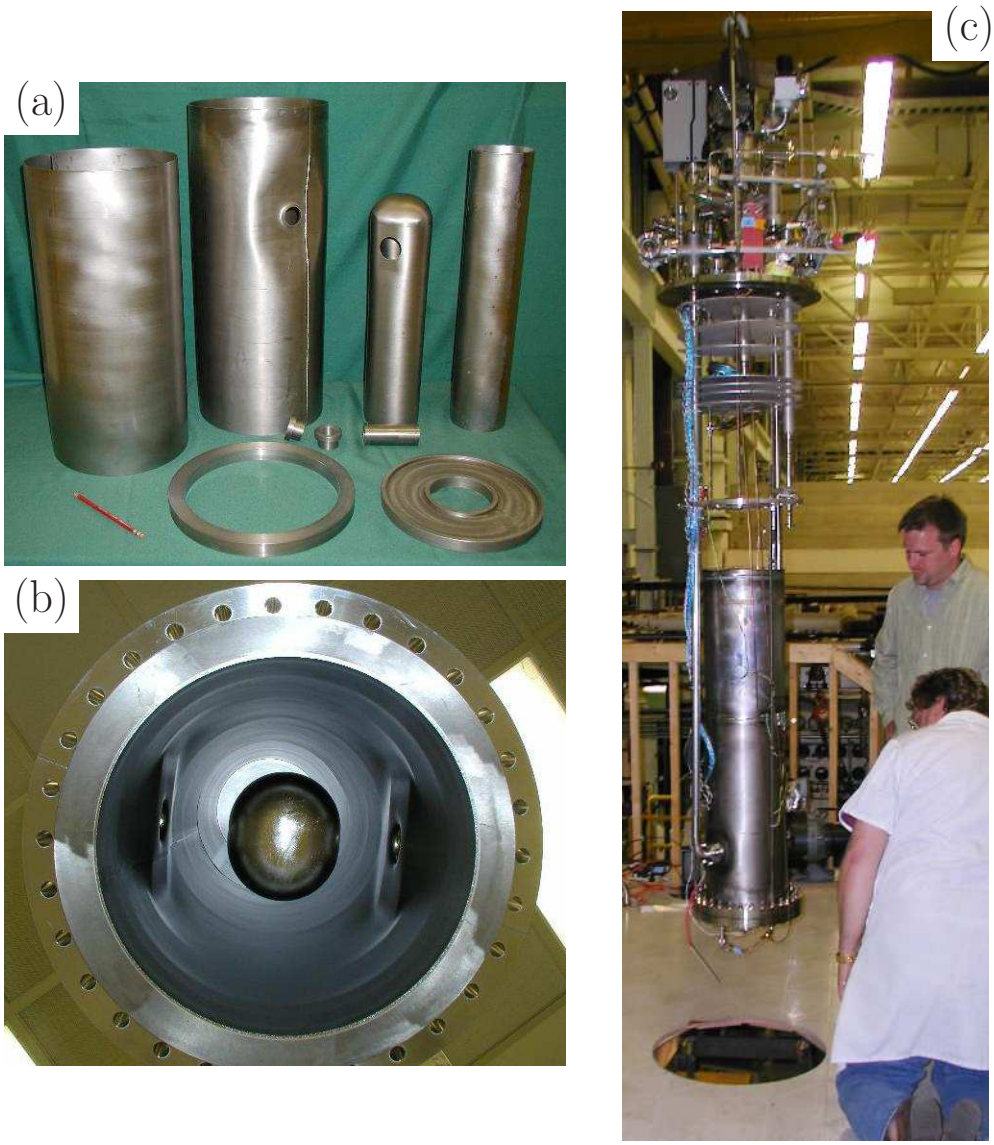

Figure 6. (a) Nb parts for $\beta = 0.085$ QWR; (b) inside view of the completed cavity; (c) cavity on the RF test stand.

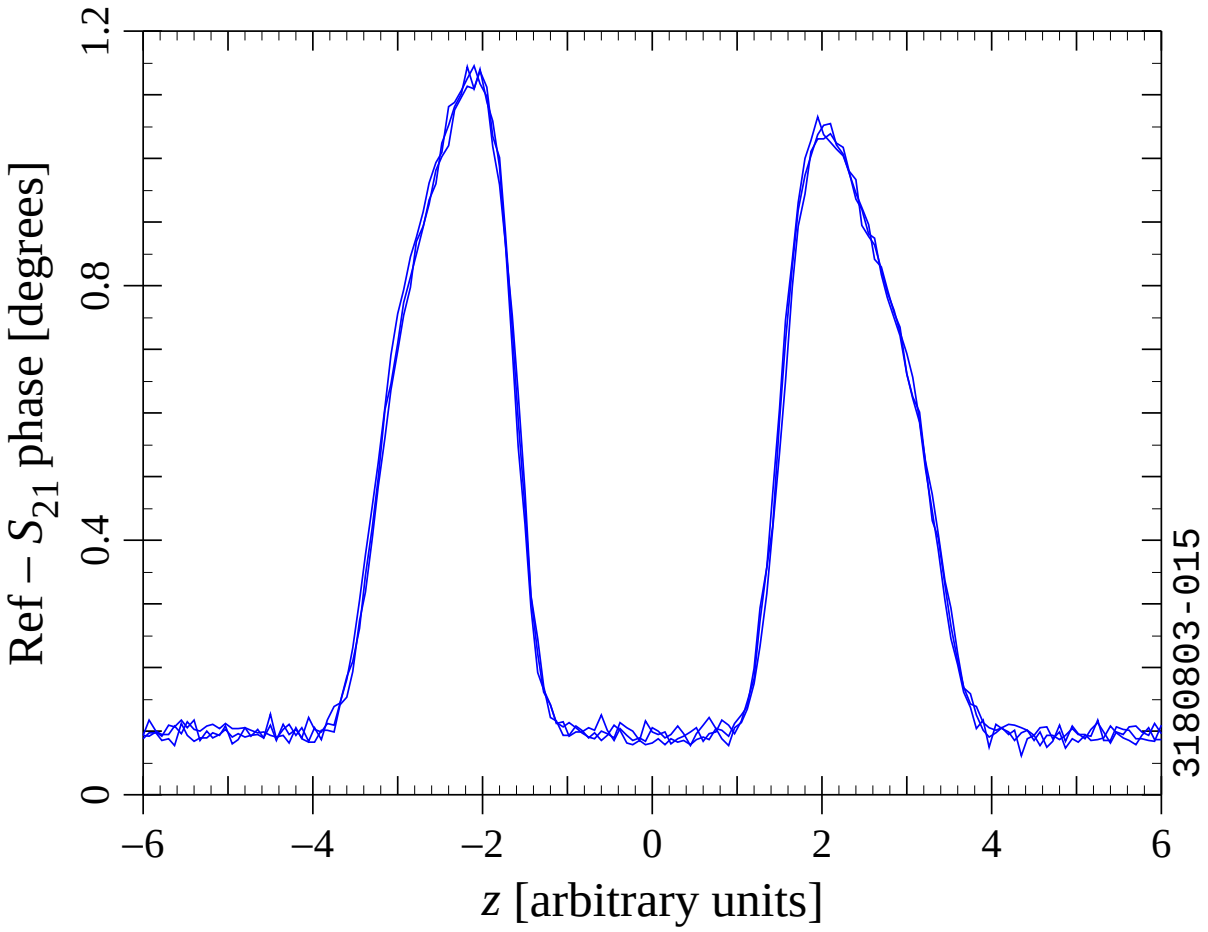

Figure 7. Bead pulls for the $\beta = 0.085$ QWR prototype.

the cavity and pick up the transmitted power signal. The input antenna length was chosen to be near unity coupling at low field at 4.2 K.

Multipacting barriers were encountered at low field. We were able to get through the barriers with 1 to 2 days of RF conditioning at 4.2 K. The barriers were not completely eliminated by conditioning; reconditioning was required in some circumstances. No conditioning was done at higher temperatures.

The first RF tests on the $\beta = 0.085$ QWR were done in September 2003 and October 2003. Results at 4.2 K and 2 K are shown in Figure 8. A field level of $E_p = 31$ MV/m was reached at 4.2 K. Above that field level, we reproducibly lost lock on the feedback loop, possibly due to thermal breakdown. A slightly higher field was reached at 2 K.

A system of mirrors was used to view the outside of the cavity with a video camera placed on top of the cryostat. At high field, the video images indicated that bubbles were being

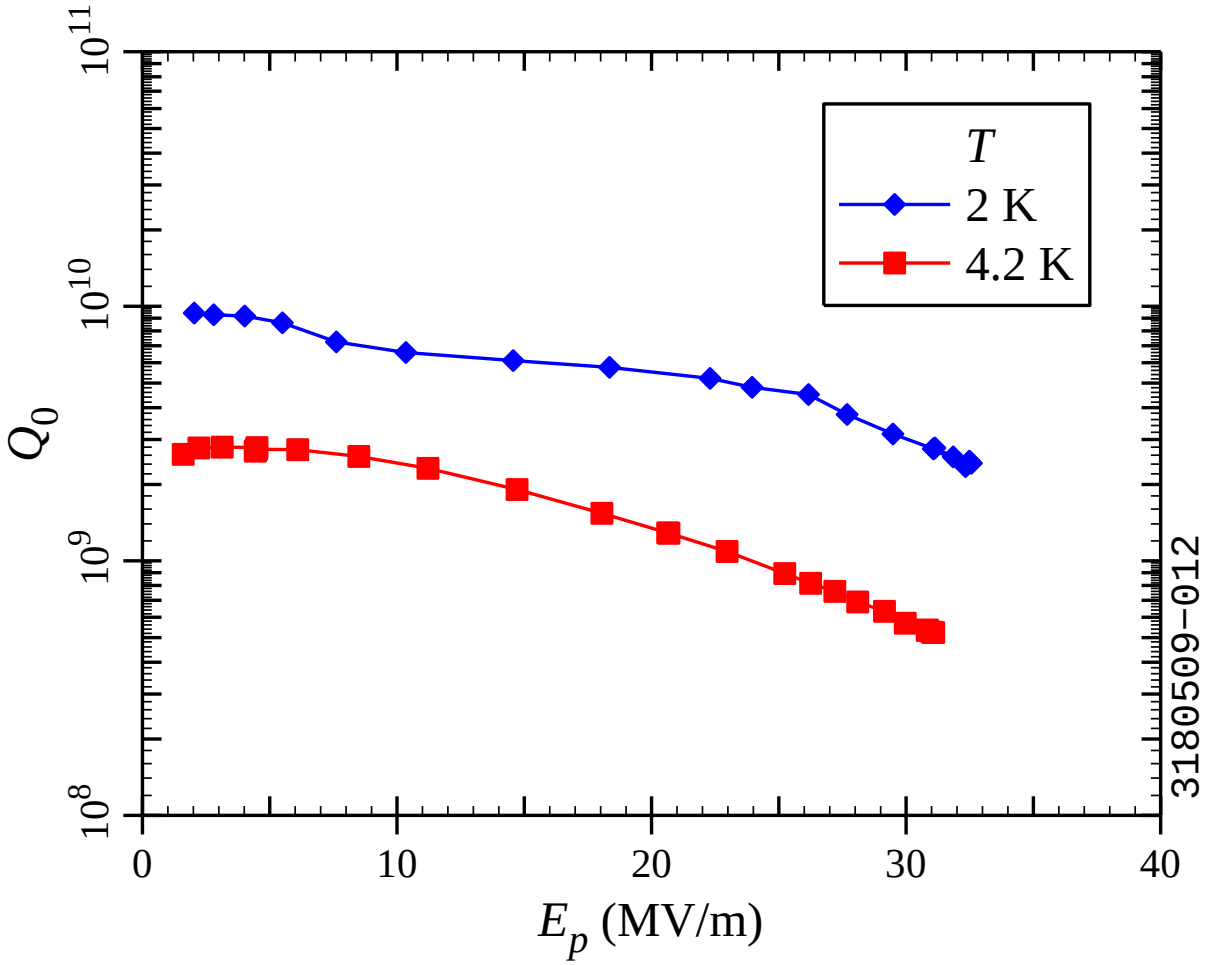

Figure 8. RF test results for the $\beta = 0.085$ QWR.

nucleated more or less uniformly near the top of the cavity, as one would expect for losses due to the magnetic field.

The low-field Q_0 value of about $3 \cdot 10^9$ at 4.2 K corresponds to an RF surface resistance of $R_s = 6.3$ nΩ; the expected contribution from the BCS term is 2.9 nΩ. The low-field Q_0 was $6 \cdot 10^9$ at $T = 1.5$ K, corresponding to a residual resistance of $R_0 = 3.2$ nΩ, in good agreement with the measured R_s at 4.2 K and expected BCS contribution.

After Dewar testing, a helium vessel was constructed around the cavity. The vessel is made of titanium. The vessel design includes a Legnaro-type frictional damper [9] inside the inner conductor to mitigate microphonic excitation of the cavity. Another Dewar test was done with the helium vessel (see section 6).

4 Magnets

Two superconducting magnets were included in the cryomodule for focussing. The first magnet is a 9 T solenoid with an integrated steering dipole. The second is a super-ferric 31 T/m quadrupole. The current is supplied to both magnets with a commercial high temperature superconductor (HTS) lead package. The solenoid was fabricated by Cryomagnetics, Inc; the quadrupole was fabricated at MSU [6].

After fabrication, both magnets were cooled down and energized to full field to magnetize the iron and steel components. The quadrupole was energized to 48 T/m at MSU; the solenoid was tested to 9 T (92.3 A) by the vendor. After warming up, the remnant field outside the cryoperm shield of the quadrupole was 0.8–2 μT, as measured with a flux-gate magnetometer; the measured remnant field of the solenoid was 0.4–2 μT.

5 Magnetic Shielding

The cavities are in proximity to the magnets when the components are installed into the cryomodule. The magnetic fields at the cavities must be limited to acceptable levels during cool down and operation to avoid degradation of the quality factor. The maximum acceptable magnetic field during cool down for the QWR and HWR cavities are 10 μT and 2.5 μT, respectively [10].

The A36 steel of the cryomodule's vacuum vessel provides some shielding of the Earth's magnetic field, which is reduced from 50 μT to 10 μT. A cryoperm mu-metal shield[1] assembled around both cavities further reduces the external field to < 0.2 μT. Cryoperm shields are assembled around both magnets to isolate the internal remnant fields.

The 9 T solenoid has reverse wound compensation coils to reduce the stray magnetic field. A reactor grade 2 mm thick niobium shield is installed around the solenoid and heat-sunk to it. When superconducting, this niobium shield traps the field inside via the Meissner effect. The final cryoperm shield traps any remaining stray field. The quadrupole's field of 0.6 T

[1] Cryoperm 10, a product of Vacuumschmelze, Hanau, Germany.

is easier to shield; the iron return yoke is not saturated, and only the cryoperm shield is needed.

6 Shielding Tests

Both magnets were tested in proximity to a cavity to make sure the magnet field did not produce any degradation in RF performance. The HWR was used for these tests because it is more sensitive to external magnetic fields than the QWR. The cavity and magnet separation distance was chosen to match that of the final assembly inside the cryomodule.

Results of cavity testing with and without the solenoid in proximity are shown in Figure 9. The squares and triangles indicate cavity tests after installation of the helium vessels, without a magnet in proximity to the cavity. The diamonds indicate the test of the HWR in proximity to the solenoid. Before this measurement, the solenoid was energised to full current; the cavity was then warmed up above the critical temperature and cooled back down; the solenoid was energised to full current again during the RF measurements. As can be seen, no degradation in RF performance is observed due to the operating field or remnant field of the magnet. Likewise, no degradation in performance was observed in RF tests of the HWR with the quadrupole in proximity to it.

7 Cryomodule Design

A drawing of the prototype cryomodule is shown in Figure 10. The module was designed to accommodate the $\beta = 0.085$ QWR, the $\beta = 0.285$ HWR, the 9 T solenoid, and the super-ferric quadrupole. Selected cavity, magnet, and cryogenic parameters are given in Table 1.

Beam dynamics simulations indicate that cavity alignment tolerances for the low-β linac are ± 2 mm, while magnet alignment tolerances of ± 1 mm are needed for efficient beam transport with minimal emittance growth [11]. All beam line components are rigidly aligned on a titanium rail with optical fiducials at the ends and center of the rail that can be viewed while at operating temperature. The cold mass is assembled in a Class 100 clean room. The cavity and beam line vacuum are isolated from the insulating vacuum using metal seals. Component alignment is done using push-pull bolts that allow ± 3 mm adjustment. The cold mass is hung from the vacuum vessel top plate using 4 nitrogen-alloyed stainless steel support links[2] with ball and socket connections at both ends. A stainless steel helium manifold is welded to the beam line components, with bi-metal transitions to the cavities' Ti helium vessels. The vacuum vessel is made from low carbon steel plate. Pins secure the cold mass to the vacuum vessel during transportation.

[2]Nitronic 50, a product of Tripyramid Structures, Westford, MA.

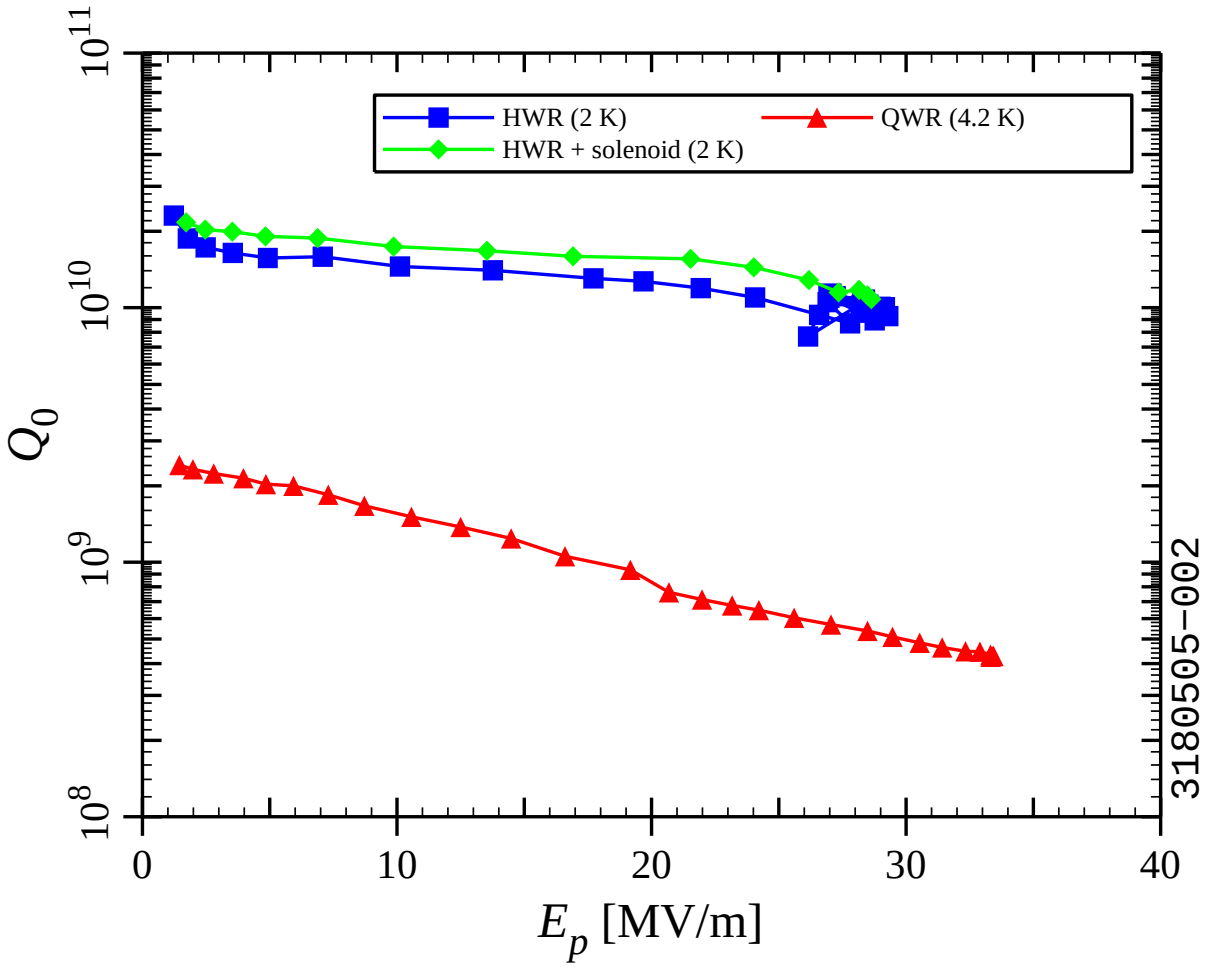

Figure 9. RF test results for the HWR, HWR in proximity to the solenoid, and QWR.

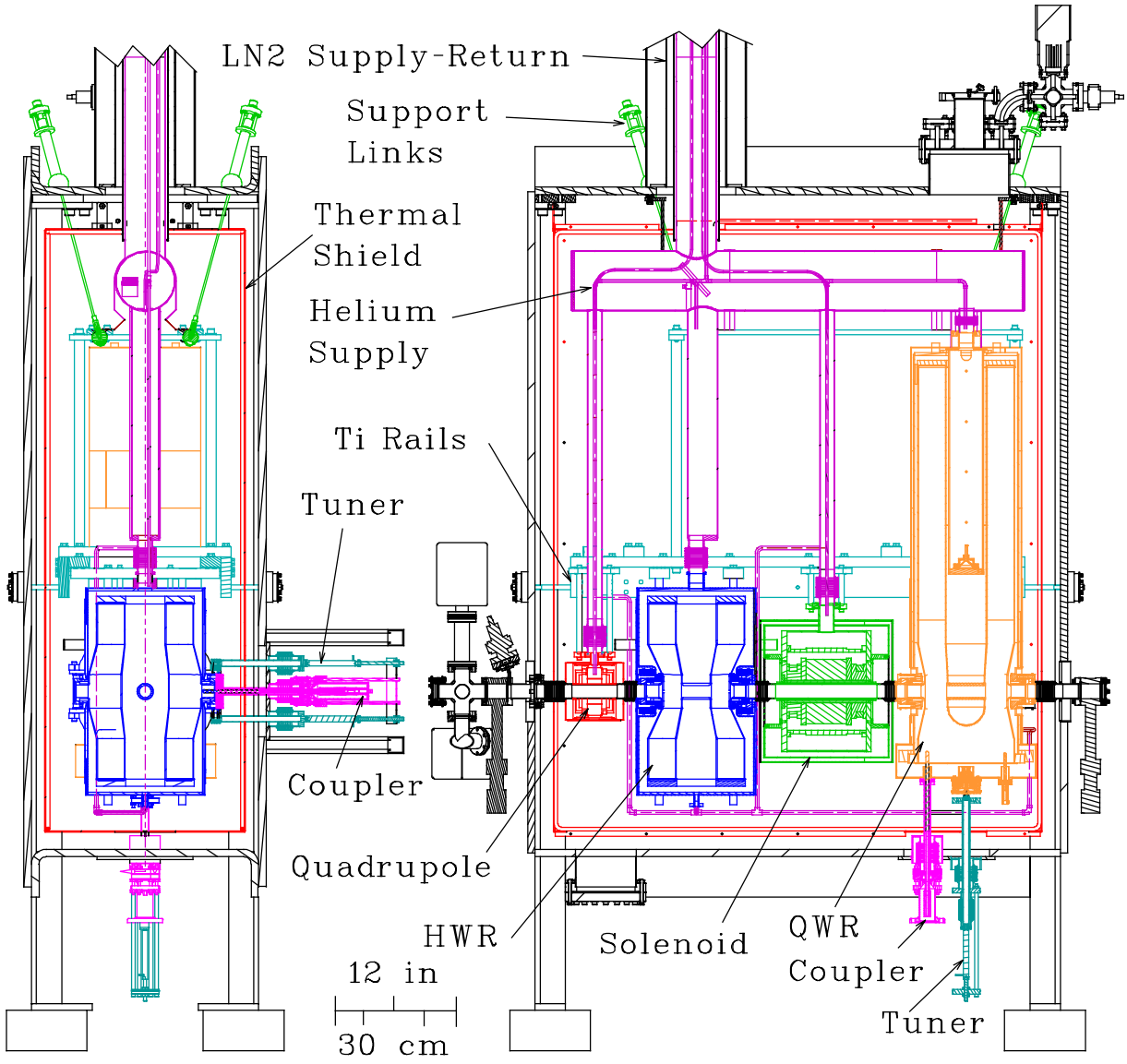

Figure 10. Sectional views of the prototype cryomodule.

Table 1. Design parameters for the cryomodule, cavities, and magnets; V_a is the accelerating voltage (transit time included), E_p is the peak surface electric field, B_p is the peak surface magnetic field, and Q_0 is the cavity intrinsic quality factor. The RIA design goals for the cavities are given. Note that the FRIB design goals are a bit different (for example, the FRIB design field level is $E_p = 30$ MV/m for both cavities).

Cavity	QWR	HWR
Frequency	80.5 MHz	322 MHz
$\beta = v/c$	0.085	0.285
Beam Current	0.16 mA	0.35 mA
V_a	1.18 MV	1.58 MV
Max Beam Power	0.16 kW	0.48 kW
E_p	20 MV/m	25 MV/m
B_p	47 mT	69 mT
Design Q_0	$5 \cdot 10^8$	$5 \cdot 10^9$
RF Loss	6.7 W	2.5 W
RF input power	< 1 kW	
Magnet	Quadrupole	Solenoid (Dipole)
Effective length	50 mm	100 mm
Aperture	40 mm	40 mm
Strength	31 T/m	9 T (0.01 T·m)
Turns	78	16 813 (40)
Current	63 A	68 A (50 A)
Heat load to He	QWR	HWR
Input coupler	0.40 W	0.60 W
Tuner	0.63 W	0.38 W
Total/RF off	6 W	
Total/RF on	15.2 W	
Cryomodule		
77 K shield load	< 100 W	
Length	1.54 m	
Cold mass	310 kg	
Total mass	2000 kg	

7.1 RF Couplers

The RF input couplers for the QWR and HWR were designed using a commercially available electrical feed-through [12]. The outer conductor is 0.5 mm thick 304 stainless steel with 10 μm copper plating and does not require helium gas cooling. The couplers are probe-type couplers, with the probe length chosen to achieve the desired coupling strength. For simplicity, the coupling strength is fixed. The QWR and HWR couplers were conditioned to 1.1 kW and 2 kW, respectively. Figure 11 shows a drawing of the coupler and a photograph of the conditioning set-up. After conditioning, the couplers were stored in the Class 100 clean room until assembly onto the cryomodule's cold mass.

Both cavities include probe-type pick-up couplers to monitor the RF field amplitude. The pick-up couplers' feed-throughs are inside the cryomodule insulation vacuum.

7.2 Tuners

The tuners are shown in Figure 12. The QWR is tuned by mechanically adjusting the distance between the bottom plate and the inner conductor nose. The tuner presses against the plate, which acts as a diaphragm, and the helium vessel, which counters the applied reaction forces. The force on the plate is always upward-directed, which reduces backlash. The frequency tuning of the HWR is done by mechanically compressing the cavity, with the forces applied axially at the beam tube flanges. Machined flex-joints are used to avoid backlash. Both tuners use an external piezoelectric actuator for fine tuning and a screw drive mechanism for coarse tuning. At room temperature, the measured ranges of the coarse tuners were $+0/-2.5$ kHz for the QWR and $+40/-80$ kHz for the HWR.

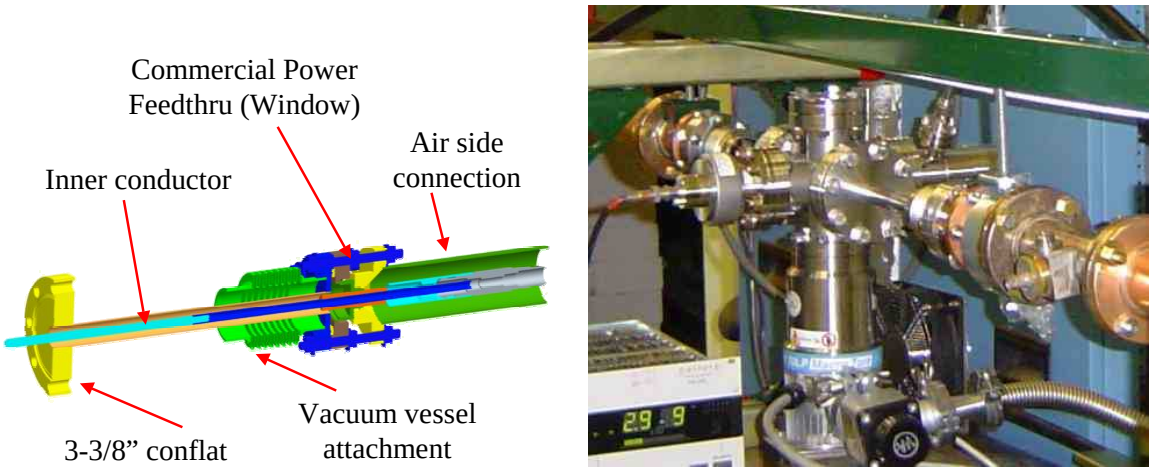

Figure 11. Left: isometric drawing of input coupler. Right: photograph of coupler conditioning stand.

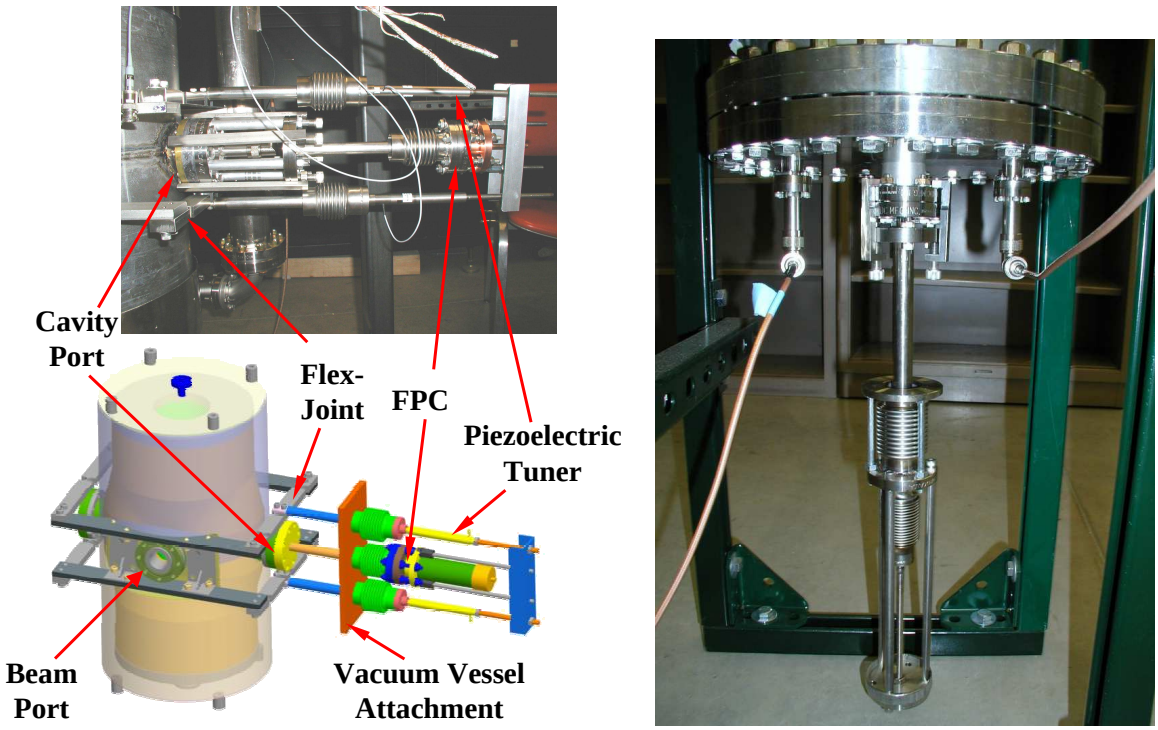

Figure 12. Left: isometric drawing and photograph of HWR tuner. Right: photograph of QWR tuner.

7.3 Cold Box

A schematic diagram of the cold box and cryomodule is shown in Figure 13. A drawing and photograph of the cold box are shown in Figure 14. The 4 K helium from the cryo-plant enters the box and passes through the 2 K sub-cooler. Next, the helium passes through a controlled Joule-Thomson (JT) valve and into a phase separator. During cool-down, the valve allowing gas to leave the phase separator is closed, speeding the cool-down by forcing all gas and liquid to be delivered to the cavities. Once steady state is achieved, the warm gas return is closed and the cold gas return is opened. Helium boil-off gas leaves the module via the manifold, exiting via the 2 K heat exchanger. The heat exchanger cools the incoming liquid at 4 K using the exiting gas at 2 K; it uses a stainless steel tube with radial aluminum fins. The HTS leads are placed inside the helium exit gas pipe, so that incoming heat from the lead wires is removed by the outgoing gas before it reaches the components at 2 K. The cold box is directly above the HWR. A view-port was added over the helium connection to allow a direct line of sight into the HWR; a mirror allows sighting down the helium manifold.

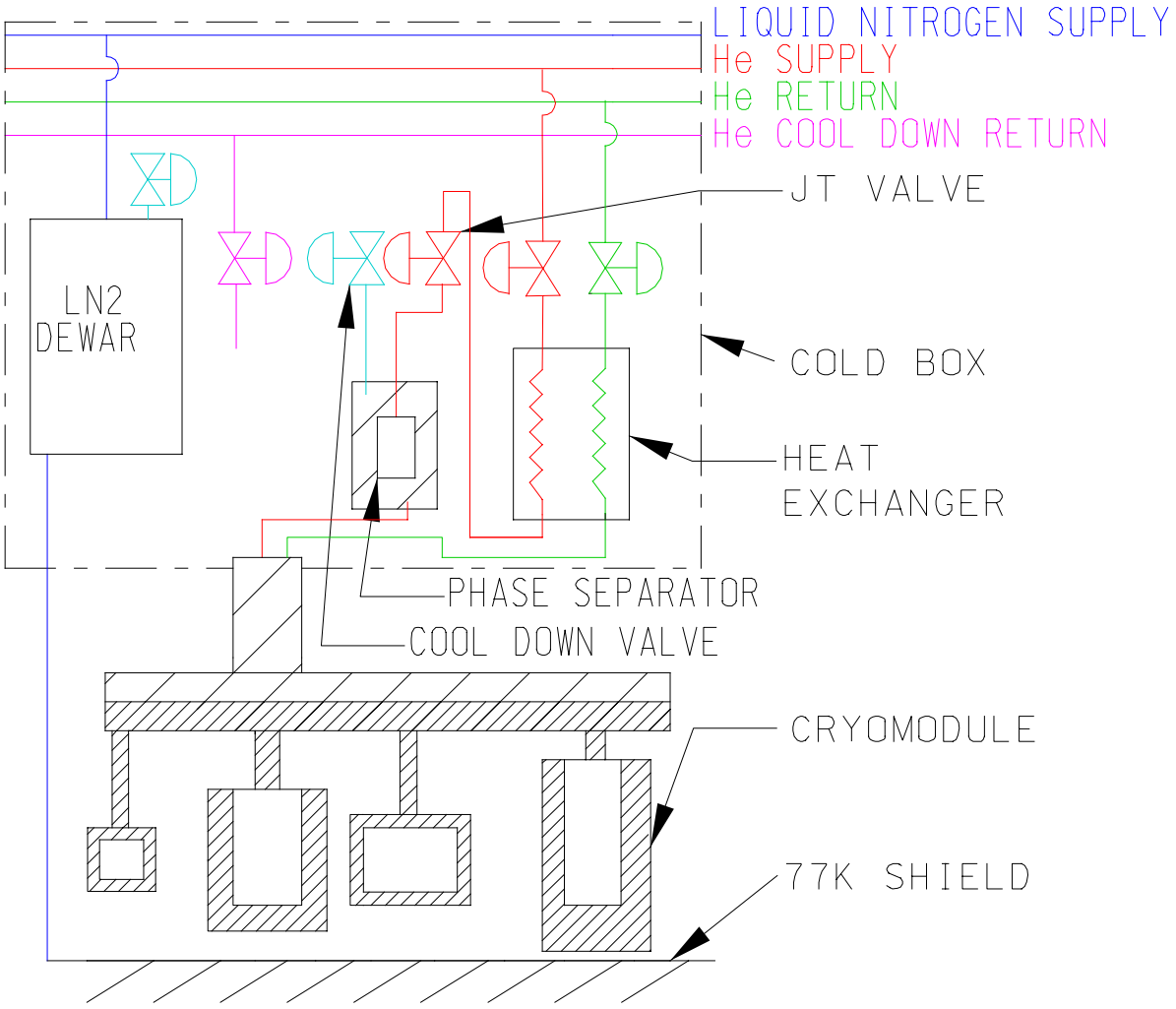

Figure 13. Schematic of cold box and prototype cryomodule.

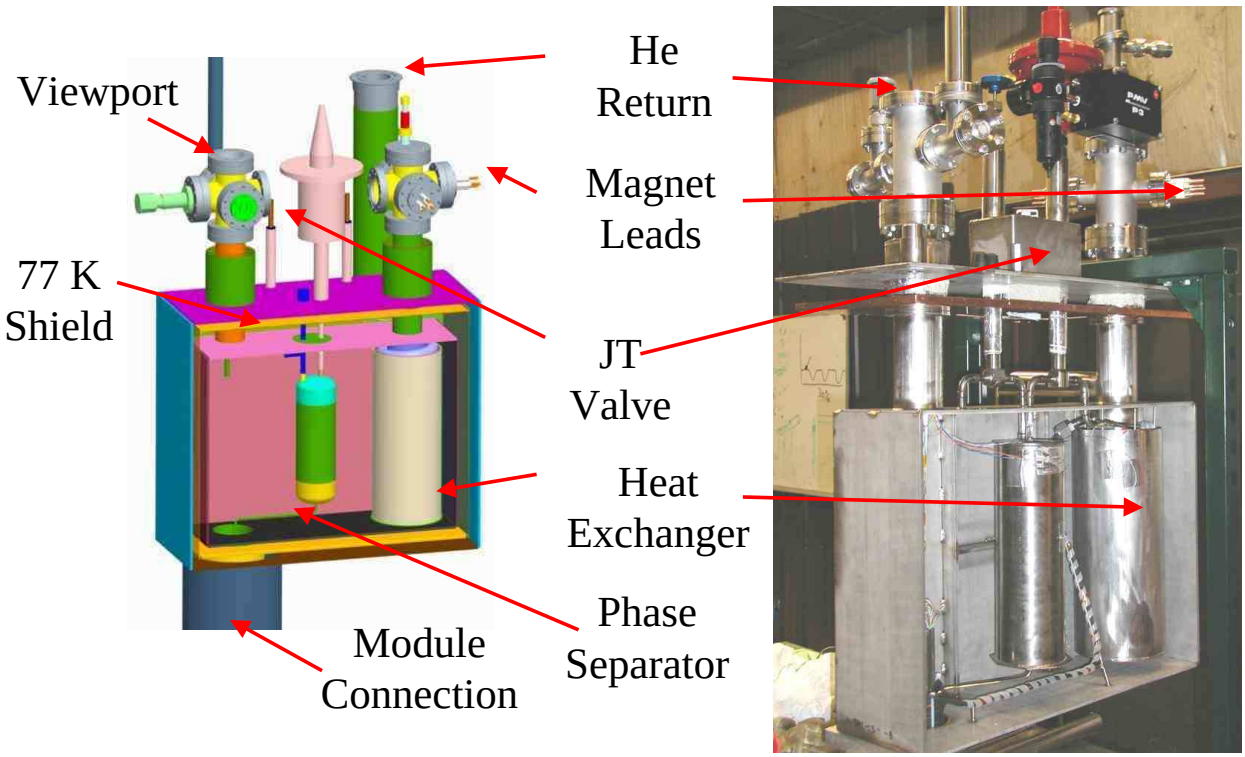

Figure 14. Left: isometric drawing of cold box. Right: photograph of partially assembled cold box.

8 Cryomodule Fabrication

In preparation for assembly of the cryomodule, the cavities were etched in the chemistry facility and rinsed with high-pressure ultra-pure water in the class 100 clean room. The superconducting magnets were cleaned and their beam tubes were rinsed with high-pressure water in the clean room. The cavities and magnets were attached to the alignment rails and the beam line vacuum chamber was pumped out and hermetically sealed in the Class 100 clean room. Figure 15 shows the finished cold mass assembly in the clean room.

The cold mass was removed from the clean room for assembly of the cryomodule. The cryomodule assembly includes the magnetic shielding for the cavities and magnets; support links for the cold mass; a 77 K shield made of copper sheet cooled by copper tubing; multi-layer insulation; the steel vacuum vessel; and the cold box. The completed cold box was tested prior to being connected to the cryomodule. Photographs of the cryomodule assembly sequence are shown in Figure 16.

9 Cryomodule Testing

Testing of the low-β cryomodule began in August 2007, ending in July 2008.

Figure 15. Cold mass assembly on titanium alignment rails inside the clean room. From left: QWR with RF coupler, solenoid with Nb shield, HWR with upper and lower cryoperm shield pieces, and quadrupole.

9.1 Cool-Down

The cryomodule was cooled down several times. One major concern during cool-down was to ensure that the cavities temperatures did not dwell between 150 K and 30 K for extended periods due to the risk of surface hydride formation ("Q disease"). Some experimentation was needed to determine the best cool-down procedure. Ultimately, nitrogen pre-cooling with the 77 K shield was done for several days before the liquid helium cooling was started, and the liquid helium flow rate was kept as low as possible to transfer the heat as efficiently as possible. The experience with cooling down is being used to guide the design of future cryomodules, which will have improved instrumentation and better heat exchange.

9.2 Static Heat Leak

The static heat leak of the cryomodule was measured from the rate of boil-off of liquid helium with the supply valve closed, using a level sensor to measure the boil-off rate. The measured static heat leak at 4 K was 4.5 W $\pm$ 1.2 W, which is a bit smaller than the design value of 6 W from Table 1. A more realistic thermal analysis was done for the cryomodule, giving a predicted value of 5.2 W, which is a bit more consistent with the measured value.

9.3 RF Testing of QWR

RF testing of the QWR was done first with a direct connection from the RF amplifier to the coupler, and then with a sliding short to set up a standing wave on the rigid copper coaxial transmission line. The sliding short configuration provided less mismatch and made it easier to infer the intrinsic Q of the cavity (Q_0) from the RF measurements. Simple loop couplers were used to couple into the transmission line through the short and monitor the field in the

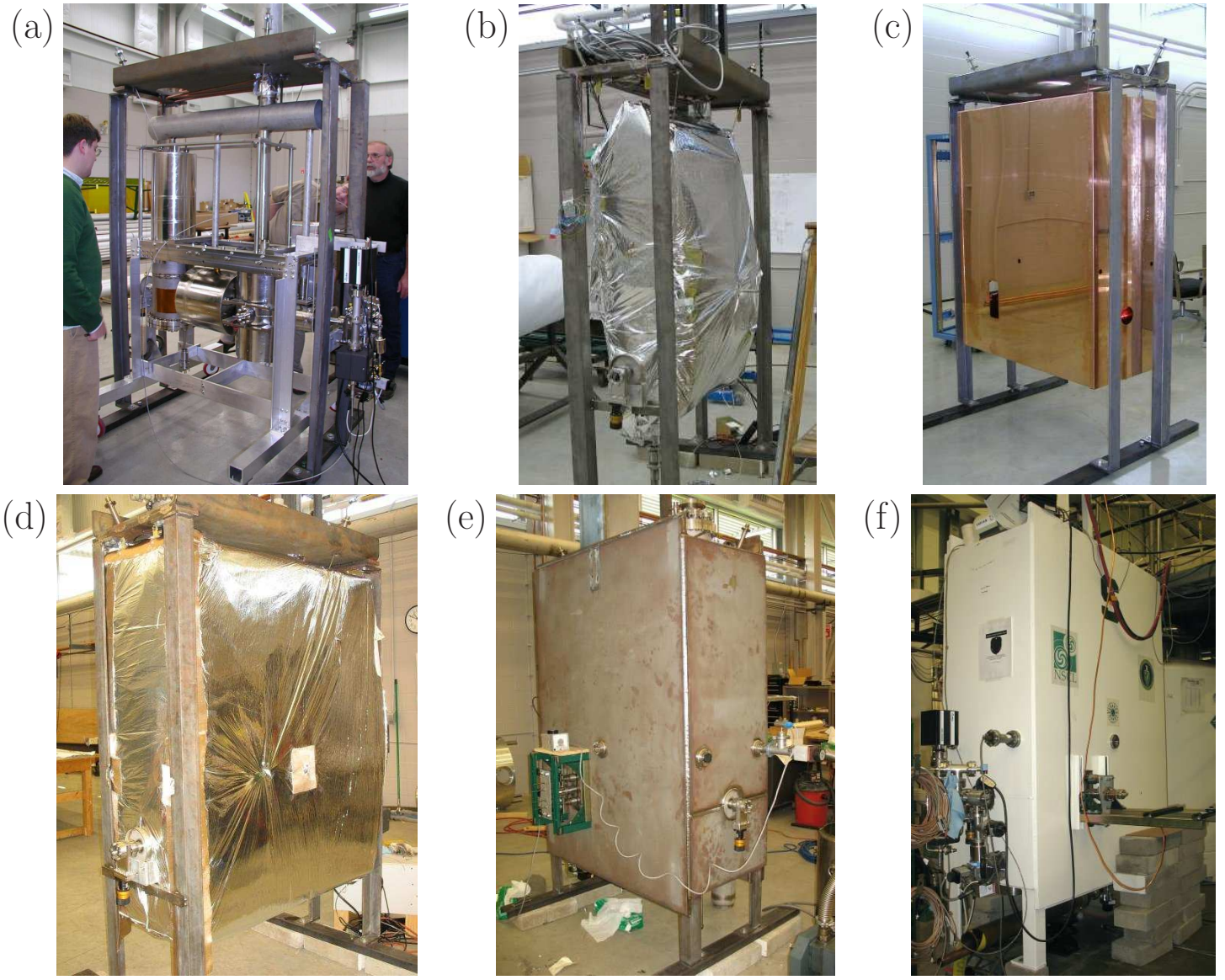

Figure 16. Construction of the low-β test cryomodule: (a) cold mass hanging from top plate; (b) inner multi-layer insulation; (c) 77 K shield; (d) outer multi-layer insulation; (e) vacuum vessel; (f) cryomodule under test.

line. The losses in the transmission line were estimated with additional RF measurements, and were subtracted out when calculating the cavity intrinsic Q.

The measured input coupling strength was $Q_{ext} = 4.5 \cdot 10^6$ with a direct connection. With the sliding short set to minimise losses in the copper, the measured Q_{ext} was $1.4 \cdot 10^9$.

Multipacting barriers were observed at low field. With conditioning, we were able to get beyond the barriers, but we were not able to eliminate them.

RF conditioning and helium processing were done to mitigate field emission. Figure 17a shows the measured RF performance of the QWR at various stages of the RF testing. Before conditioning, the maximum field reached at 4.5 K was about $E_p = 25$ MV/m (black squares). After several shifts of pulsed RF conditioning at 4.3 K to 4.5 K, some improvement in the high field performance was observed (red diamonds). Additional pulsed conditioning at 2 K produced some further improvement (green triangles). Helium processing at or below 2 K yielded a more significant increase in Q_0 at high field (blue triangles). X-rays were still observed at high field after helium processing, although the x-ray flux was smaller.

The introduction of helium gas into the cavity for helium processing worsened the multipacting barriers. Some reconditioning of the barriers was required after the helium processing.

Figure 17b shows the measured RF performance of the QWR at two different temperatures after helium processing. The highest field reached in the QWR testing was $E_p \approx 33$ MV/m.

Figure 18 shows the measured performance of the QWR after He processing as compared to the performance in the Dewar test. The performance in the cryomodule is similar to the performance in the Dewar test.

9.4 RF Testing of HWR

As with the QWR, most of the RF testing of the HWR was done with a sliding short to reduce the mismatch. Likewise, the losses in the transmission line were estimated and subtracted out when calculating the cavity intrinsic Q. At 2 K, the losses in the transmission line were large relative to the losses in the cavity, so that the errors in the calculated Q_0 values were large, making it difficult to infer Q_0 from the RF measurements.

Multipacting barriers were observed at low field. We were able to get through them with RF conditioning.

RF conditioning was attempted to reduce field emission. Some performance degradation was observed when the HWR was operated at high field for extended times. Helium processing was attempted after the performance degradation was observed. The helium processing reversed the performance degradation. However, the introduction of helium gas into the cavity worsened the multipacting barriers, as was the case for the QWR. Several hours of conditioning were required to get through the barriers after the helium gas was pumped out. The introduction of helium gas into the beam line vacuum for conditioning of the HWR was also observed to worsen the multipacting barriers in the QWR.

RF measurements on the HWR in the cryomodule are compared to Dewar results in

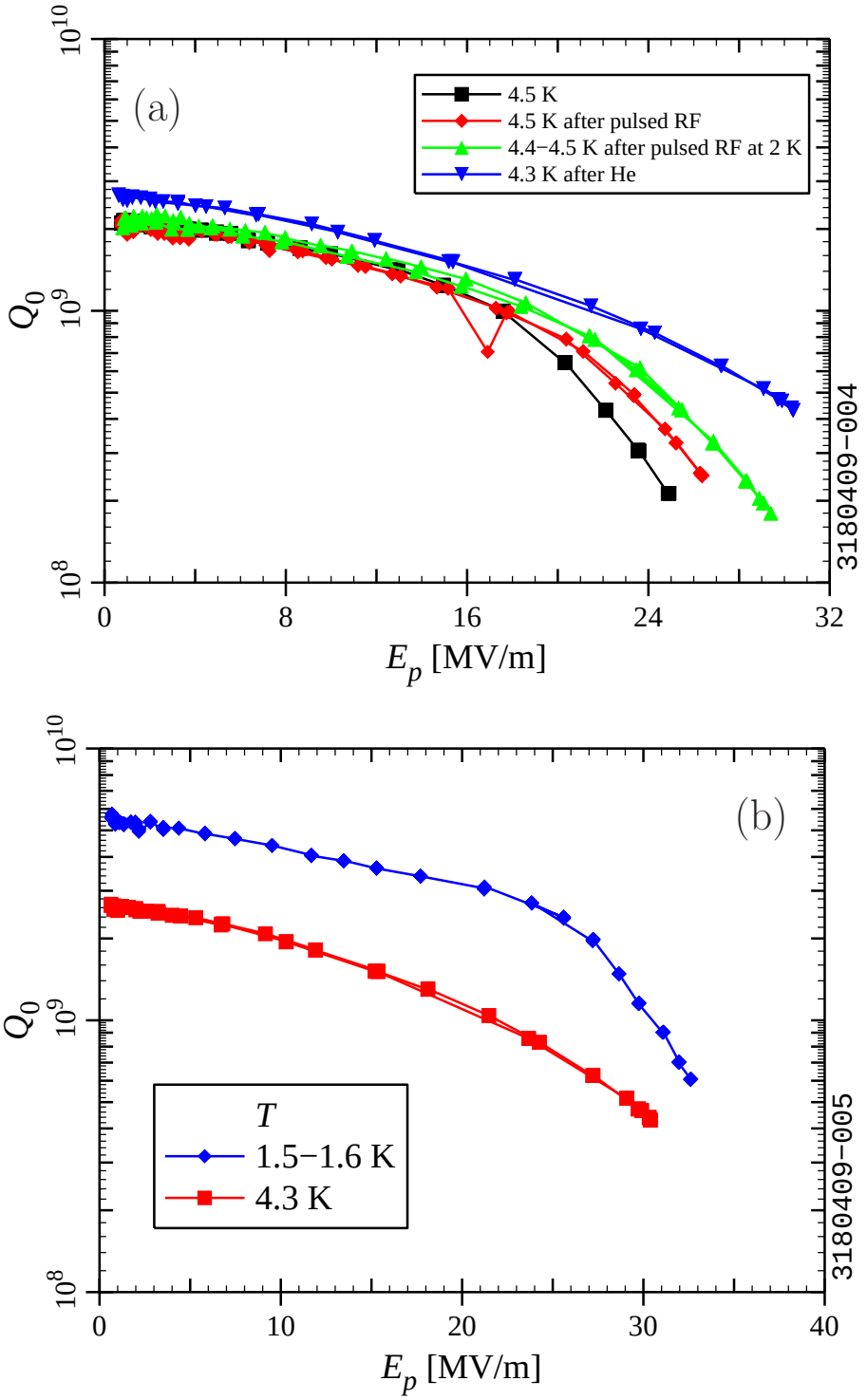

Figure 17. (a) Conditioning of the QWR to reduce field emission. (b) Comparison of QWR RF test results at 2 different temperatures after helium processing.

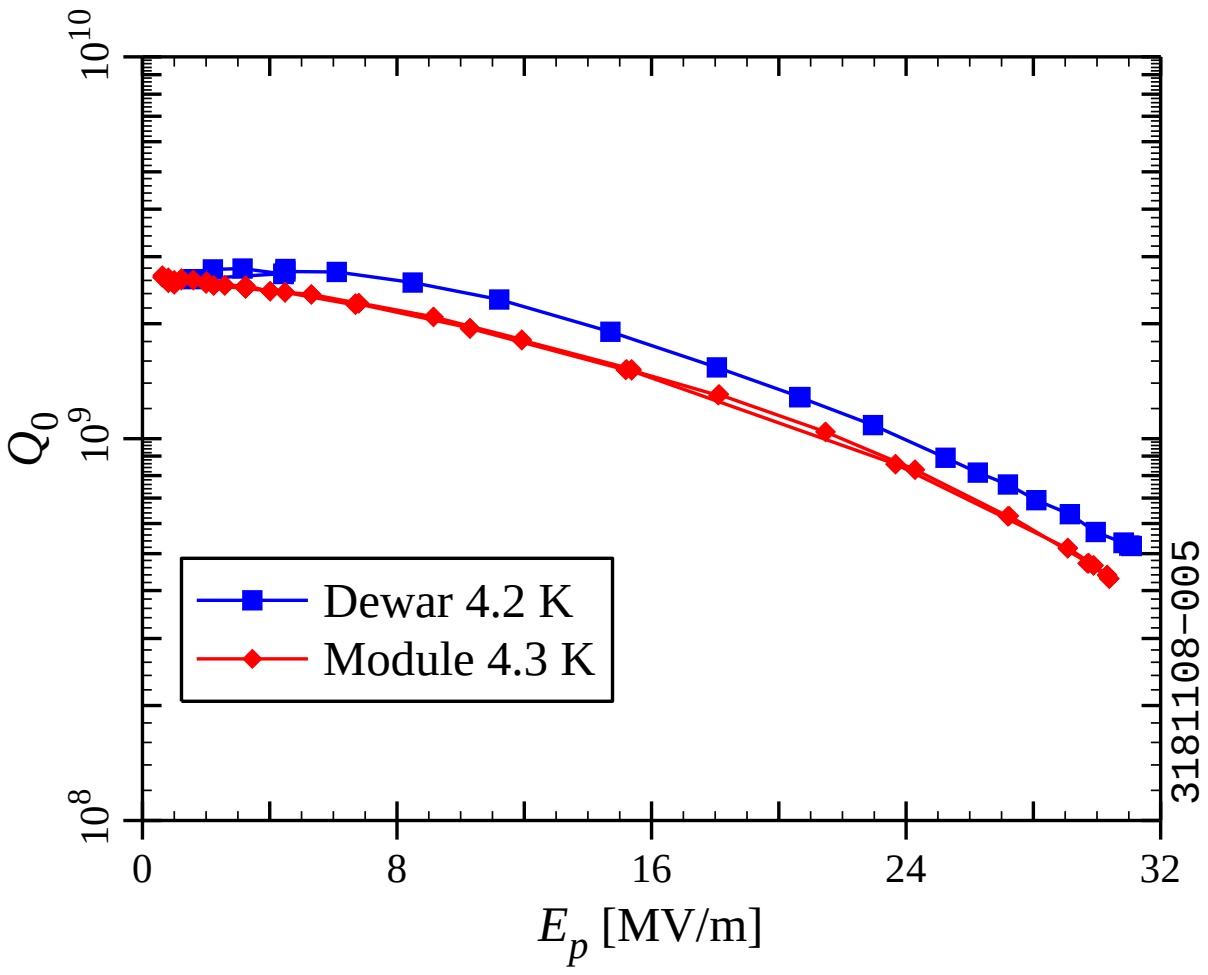

Figure 18. RF test results for the $\beta = 0.085$ QWR: comparison of Dewar test and cryomodule test. The cryomodule measurements were done after solenoid operation, temperature cycling, and He processing.

Figure 19. The cryomodule measurements at 4.2 and 4.3 K are in reasonable agreement with the Dewar test results. The cryomodule measurements at 3 K are also reasonably close to the Dewar results, except that the error in the measured Q_0 values starts to become large at low field, because the losses are becoming dominated by the transmission line.

Measurements were also done in the cryomodule at 2 K, but the uncertainty in the Q_0 values was large enough to make it difficult to interpret the results. We estimate that the highest field we reached at 2 K was $E_p = 35$ MV/m. In future cryomodule testing, calorimetric measurements should provide a way to measure the power dissipation in the cavity independently of the RF power measurements. (Some calorimetric measurements were attempted in the low-β cryomodule test, but we did not spend enough time on them to establish confidence in the results.)

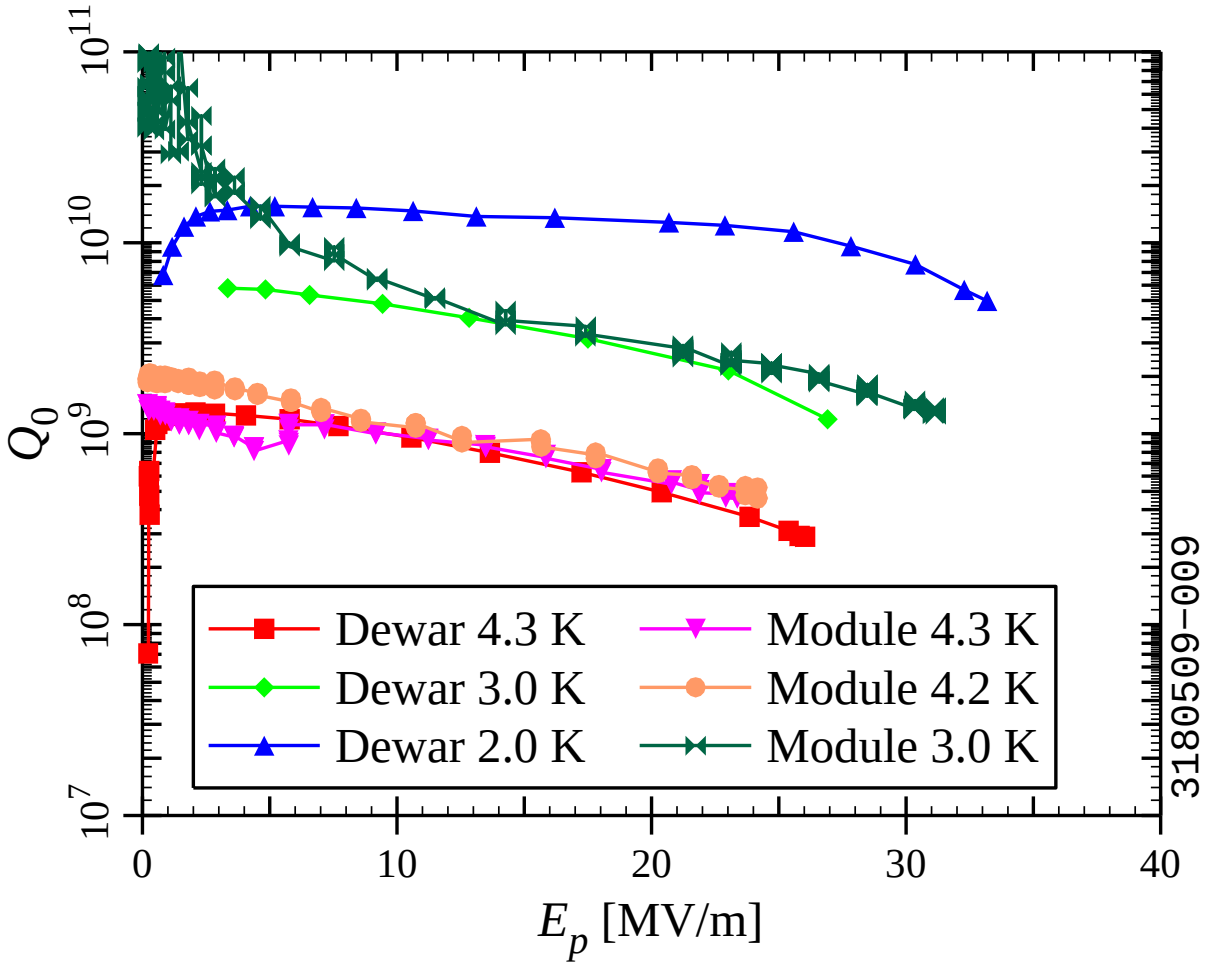

Figure 19. RF test results for the $\beta = 0.285$ HWR: comparison of Dewar test and cryomodule test. The cryomodule measurements were done after operation of the solenoid and temperature cycling of the cryomodule, but before helium processing.

9.5 X-Ray Spectrum Measurements

Bremsstrahlung X-rays were produced by the QWR and HWR at high RF field due to field emission electrons being accelerated by the RF electric field and impacting the wall of the cavity. X-ray spectra were measured several times during RF testing of the QWR and HWR to check the RF field amplitudes inferred from RF power measurements.

The X-ray energy spectrum was recorded with a germanium gamma-ray detector connected to a multichannel analyzer. The detector was shielded on its sides with 50 mm thick lead bricks to reduce background from undesired sources of gamma rays. As expected, the X-ray output from the cavities increased sharply as the RF drive power increased. To reduce the counting rate in the detector, metal energy absorber plates were inserted in front of the

detector for measurements with high flux rates. Tungsten and lead absorbers were used for this purpose. The thickest absorber was 50 mm of lead. Initial measurements were done with the detector near the cryomodule, approximately 0.3 to 0.4 m from the source of the X-rays. Some of the later measurements were done with the detector farther away to reduce the X-ray flux. X-ray counting was typically done for several minutes, while keeping the RF field approximately constant.

An ionisation chamber located near the cryomodule was used to independently monitor the X-ray flux. The dose rate measured by the ion chamber during the X-ray spectrum measurements was less than or equal to 80 mrem per hour. Meaningful X-ray spectra could still be measured with the germanium detector even when the ion chamber reading was below its minimum reading of about 1 mrem per hour.

To verify the RF field amplitude measurements, the X-ray end-point energy was compared to the RF voltage inferred from RF power measurements. This technique has been used successfully in the past at NSCL to measure the dee voltages in the cyclotrons, and the voltage on the deflecting plates of the RF separator. These devices produced voltages between 50 kV and 150 kV. The same technique has been used for superconducting cavities as well.

In the present case, we assume that electrons leaving one side of the gap are accelerated rapidly and arrive on the opposite side of the gap in a time that is short compared to the RF period (12.4 ns for the QWR and 3.1 ns for the HWR). For the QWR, this condition is satisfied for the measured voltages (400 kV and above). The estimated correction to the energy due to finite transit time (about 0.5 ns for 10 cm distance) is less than 3% at 400 kV, and is neglected.

Figure 20 shows a spectrum measured while operating the HWR at $E_p \approx 25.5$ MV/m. A background measurement (taken with the RF power turned off) is also shown, along with the difference spectrum (signal minus background). The signal and background should be the same (within statistical fluctuations) for energies above the X-ray end-point. The estimated end-point energy for the case shown in Figure 20 is 988 keV, indicated by the dotted line.

The end-point energies and voltages inferred from RF measurements are compared in Figure 21. A number of measurements on the QWR are shown; measurements were done at various times during RF testing and conditioning. A few values for the HWR are also shown; these were measured near the end of the cryomodule test. A few of the values are "corrected" values, in which a more careful estimate of the end-point energy was done after the data were recorded. As can be seen, the corrected values have a slightly lower end-point energy than the uncorrected values.

The horizontal axis in Figure 21 shows the voltage difference between the inner and outer conductor calculated from the RF power measurements (we assume no electrons are accelerated across both gaps). Values should lie on the black line if the X-ray measurements agree with the RF measurements. Most of the values for the QWR agree within 10% or so. For the HWR, the X-ray end-point energies suggest that the voltage is about 15% higher than indicated by the RF power measurements.

The agreement between the X-ray end-point energies and the RF amplitude calculated

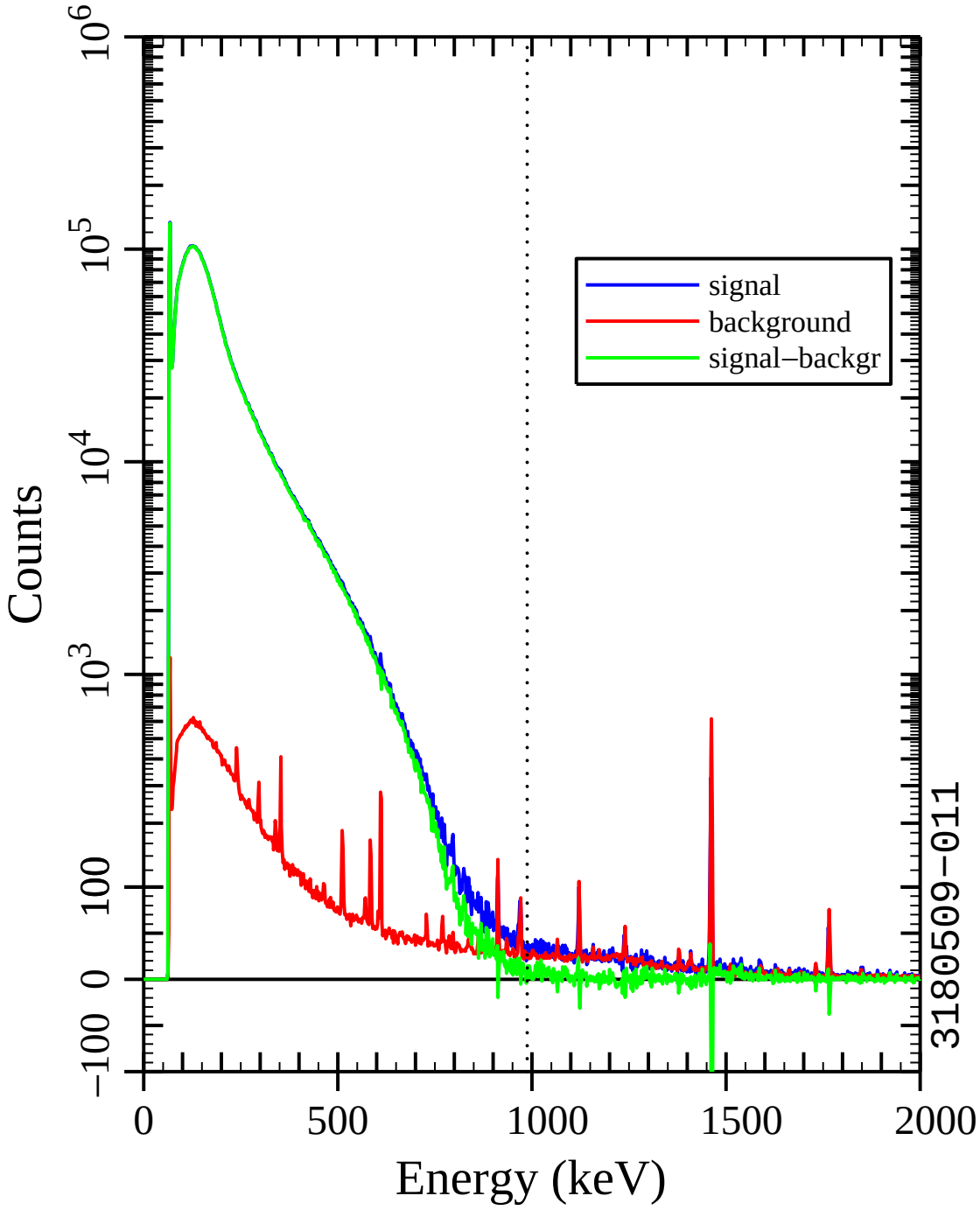

Figure 20. X-ray spectrum measurement for the HWR for $E_p \approx 25.5$ MV/m. The dotted line indicated the estimated X-ray end-point energy. The measurements were done after operation of the solenoid and temperature cycling of the cryomodule.

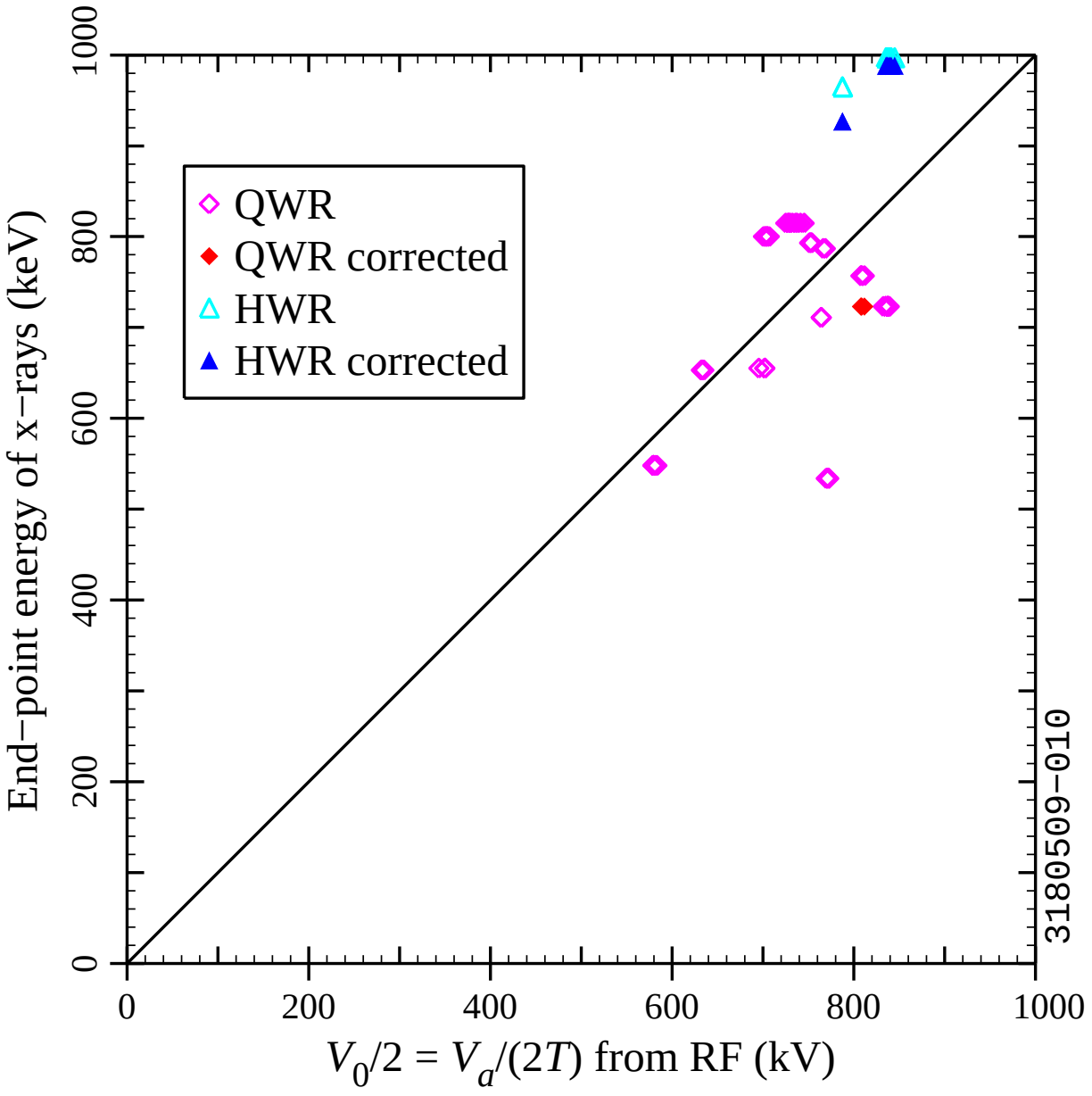

Figure 21. Comparison of RF voltage inferred from RF power measurements (horizontal axis) and RF voltage inferred from X-ray spectrum measurements (vertical axis) for the QWR and HWR.

from RF power measurements is reasonably good. Hence, we conclude that the RF power measurements are reasonably accurate.

9.6 Solenoid Operation

No degradation in cavity performance was observed with the solenoid at full field. A decrease in the low-field Q_0 of the QWR was observed near the end of one cool-down, possibly due to the Meissner shield becoming warm with the solenoid energised. The cavity performance recovered after the cryomodule was warmed to room temperature and re-cooled.

9.7 RF Couplers

The RF input couplers' performance was adequate for the cryomodule test. However, there was some concern about the risk of stressing the feed-through ceramic during cryomodule assembly or assembly of the air side transmission line (fortunately, neither feed-through failed).

An increase in the cavity pressure was observed when driving the HWR at high forward power. As a consequence, we did not attempt to operate the HWR at high field for extended periods.

In light of the experience during the cryomodule assembly and testing, a more robust feed-through design with additional instrumentation was selected for future RF input couplers.

In the first cool-down of the cryomodule, the signal from the pick-up coupler of the QWR dropped abruptly. In a second trial cool-down, this problem was determined to be due to the RF cable inside the cryomodule insulation vacuum. The cable was replaced, which corrected the problem.

9.8 Tuners

The tuners were operated over their full range. The QWR tuner was operated at 4.3 K to 4.5 K with a stepping motor. The tuning resolution was about 1.8 Hz per step, corresponding to about 40 μm per step. No statistically significant change in the input coupling strength or pick-up coupling strength was observed due to the displacement of the tuning plate.

The HWR tuner was operated at 4.5 K and 2 K. The tuner was adjusted manually for the measurements.

9.9 Frequency Issues

The pressure sensitivities of the QWR and HWR were measured before and after installation of the cavities into helium vessels. Additional pressure sensitivity measurements were done after the cavities were installed into the test cryomodule. Measured and predicted values of pressure sensitivity are compared in Table 2. The pressure sensitivity prediction was done by E. Zaplatin (FZ-Jülich).

Table 2. Measured and predicted values of the shift in resonant frequency f with bath pressure P.

Cavity	β	Stiffened	He vessel	Location	df/dP (Hz/mbar)	
					Predicted	Measured
QWR	0.085	no	no	Dewar		−19.7
QWR	0.085	no	yes	Dewar		−7.8
QWR	0.085	no	yes	Module	−6.8	−7.3
HWR	0.285	no	no	Dewar		−198
HWR	0.285	no	yes	Dewar		−201
HWR	0.285	no	yes	Module		−147

The magnitude of the measured pressure sensitivity of the QWR is reduced by more than a factor of 2 when the helium vessel is present. With the helium tank present, the pressure sensitivity is about the same in the cryomodule test as in the Dewar test. This is likely due to a reduction in deflection of the beam ports with the helium vessel present.

No significant change in pressure sensitivity is observed for the HWR due to installation of the helium vessel. However, some reduction in pressure sensitivity is observed after the HWR is installed in the cryomodule. This might be due to partial cancellation of the deflection from the outward pressure force acting on the helium vessel (there was no pressure differential between the inside and outside of the helium tank in the Dewar test).

The Lorentz detuning coefficients of the QWR and HWR were measured before and after installation of the cavities into the cryomodule. Measured Lorentz detuning coefficients are compared in Table 3. For both cavities, some reduction in the magnitude of the Lorentz detuning coefficient is observed in the cryomodule.

Table 3. Measured Lorentz detuning coefficients for the QWR and HWR.

Cavity	β	Stiffened	He vessel	Location	df/dE_p^2 [Hz/(MV/m)^2]
QWR	0.085	no	no	Dewar	−0.19
QWR	0.085	no	yes	Module	−0.13
HWR	0.285	no	no	Dewar	−1.4
HWR	0.285	no	yes	Module	−1.1

Stiffening of the QWR and HWR are planned to reduce the pressure sensitivity. The stiffening measures may reduce Lorentz detuning as well.

Studies were undertaken to characterise the sources of frequency fluctuations. Known

sources include fluctuations in the helium bath pressure and mechanical vibrations from driving terms outside the cryomodule.

Measurements of the pressure stability of the helium system were done for various operating conditions. With the cryomodule connected to the helium gas return of the cryogenic plant, relatively large pressure fluctuations were observed, of order 50 torr to 100 torr, consistent with previous Dewar tests. Improved pressure stability could be achieved with a buffer tank (a Dewar was used for this purpose) and a control valve. A cold compressor was also plumbed into the system for some of the testing to allow for operation at lower pressure in the cryomodule. Thermo-acoustic pressure oscillations were thought to have been observed at times during the studies.

To quantify the effect of mechanical vibrations on the QWR, the bath pressure was stabilised (by disconnecting from the cryogenic plant gas return and venting the boil-off gas to the ambient atmosphere), and the RF error signal was monitored. Under these conditions, the maximum peak-to-peak frequency detuning was 5 Hz. The RMS detuning was less than 0.5 Hz. Thus, the measured fluctuations are smaller than the minimum band-width of 20 Hz planned for operating QWRs. Transfer function measurements were also done on the QWR, using a piezo-electric element to drive the tuner, or using an audio speaker to vibrate the cryomodule.

Tests of RF amplitude and phase control were done on the QWR. Some software issues were identified; follow-up tests are planned.

A feedback loop was set up using the tuner and stepping motor to compensate for shifts in the resonant frequency of the QWR due to pressure fluctuations. The RF error signal was used to drive the feedback loop. Compensation of small pressure fluctuations was done successfully with this technique.

10 Conclusion

A test cryomodule containing one quarter-wave resonator, one half-wave resonator, one solenoid, and one quadruple has been designed, fabricated, and tested. The superconducting cavities and superconducting magnets were tested prior to assembly into the cryomodule to ensure that they reached their design goals. After assembly of the cryomodule, the QWR reached the design goals at 4.5 K. The HWR reached the design field at 2 K, but it was difficult to ascertain its quality factor at 2 K because the losses were dominated by the input coupler. Pulsed conditioning and helium processing were done to reduce field emission loading of the cavities. X-ray spectrum measurements were done to check the RF amplitude inferred from RF power measurements. The measured static heat leak of the cryomodule was 4.5 W, consistent with the design goal. Some modifications to the design of the cryomodules and auxiliary components are being made in light of the experience with the test cryomodule.

11 Acknowledgments

We wish to thank all of the people who helped with cavity and cryomodule design, fabrication, and testing. The NSCL cryogenics group, operations group, and electronics group provided valuable assistance with the prototyping and testing efforts. Alberto Facco (INFN-Legnaro) provided valuable guidance for the work at NSCL. Evgeny Zaplatin (FZ-Jülich) performed a structural analysis of the quarter-wave resonator.

This work was supported by the U.S. Department of Energy under Grant DE-FG02-06ER41412.

References

[1] C. W. Leemann, "The Rare-Isotope Accelerator (RIA) Facility Project," in *Proceedings of the XX International Linac Conference*, Alexander W. Chao, Editor, Stanford Linear Accelerator Center, Stanford, California (2000), SLAC-R-561, p. 331–335.

[2] T. L. Grimm, W. Hartung, M. Johnson, R. C. York, P. Kneisel, and L. Turlington, "Cryomodule Design for the Rare Isotope Accelerator," in *Proceedings of the 2003 Particle Accelerator Conference*, Joe Chew, Peter Lucas, and Sara Webber, Editors, IEEE Publishing, Piscataway, New Jersey (2003), p. 1350–1352.

[3] T. L. Grimm, S. Bricker, C. Compton, W. Hartung, M. Johnson, F. Marti, J. Popielarski, R. C. York, G. Ciovati, P. Kneisel, and L. Turlington, "Experimental Study of an 805 MHz Cryomodule for the Rare Isotope Accelerator," in *Proceedings of the XXII International Linear Accelerator Conference, Lübeck, 2004*, Deutsches Elektronen-Synchrotron, Hamburg, Germany (2004), p. 773–775.

[4] W. Hartung, J. Bierwagen, S. Bricker, J. Colthorp, C. Compton, T. Grimm, S. Hitchcock, F. Marti, L. Saxton, R. C. York, A. Facco, and V. Zviagintsev, "Niobium Quarter-Wave Resonator Development for the Rare Isotope Accelerator," Presented at the Eleventh Workshop on RF Superconductivity (8–12 September 2003, Travemünde, Germany).

[5] T. L. Grimm, J. Bierwagen, S. Bricker, C. C. Compton, W. Hartung, F. Marti, and R. C. York, "Experimental Study of a 322 MHz $v/c = 0.28$ Niobium Spoke Cavity," in *Proceedings of the 2003 Particle Accelerator Conference*, Joe Chew, Peter Lucas, and Sara Webber, Editors, IEEE Publishing, Piscataway, New Jersey (2003), p. 1353–1355.

[6] A. F. Zeller, J. C. DeKamp, A. Facco, T. L. Grimm, J. Kim, and R. Zink, "A Superferric Quadrupole for Use in an SRF Cryomodule," *IEEE Transactions on Applied Superconductivity* **12**, p. 329–331 (March 2002).

[7] M. Johnson, J. Bierwagen, S. Bricker, C. Compton, P. Glennon, T. L. Grimm, W. Hartung, D. Harvell, A. Moblo, J. Popielarski, L. Saxton, R. C. York, and A. Zeller, "Cryomodule Design for a Superconducting Linac with Quarter-Wave, Half-Wave and Focusing Elements," in *Proceedings of the 2005 Particle Accelerator Conference*, Ch. Horak, Editor, IEEE Publishing, Piscataway, New Jersey (2005), p. 773–775.

[8] W. Hartung, J. Bierwagen, S. Bricker, C. Compton, J. DeLauter, P. Glennon, M. Hodek, M. Johnson, F. Marti, P. Miller, D. Norton, J. Popielarski, L. Popielarski, D. Sanderson, J. Wlodarczak, R. C. York, A. Facco, and E. Zaplatin, "Superconducting Quarter-Wave Resonator Cavity and Cryomodule Development for a Heavy Ion Re-accelerator," Presented at the XXIV International Linear Accelerator Conference, Victoria, BC, 2008, Paper THP033.

[9] A. Facco and V. Zviagintsev, "Completion of the LNL Bulk Niobium Low Beta Quarter Wave Resonators," in *9th Workshop on RF Superconductivity: Proceedings*, Los Alamos National Laboratory, Los Alamos, New Mexico (2000), LA-13782-C, p. 203–206.

[10] C. C. Compton, P. Glennon, T. L. Grimm, W. Hartung, L. Saxton, R. C. York, and A. Zeller, "Research Report on Efficacy of Superconducting Magnetic Elements in Proximity to RIA Superconducting Structures," Technical report, National Superconducting Cyclotron Laboratory, Michigan State University, East Lansing, Michigan (October 2004).

[11] X. Wu, M. Doleans, D. Gorelov, Q. Zhao, T. L. Grimm, F. Marti, and R. C. York, "End-to-end Beam Simulations for the MSU RIA Driver Linac," in *Proceedings of the XXII International Linear Accelerator Conference, Lübeck, 2004*, Deutsches Elektronen-Synchrotron, Hamburg, Germany (2004), p. 594–598.

[12] Adam Daniel Moblo, *Low Beta Superconducting RF Cavity Power Coupler Development for the Rare Isotope Accelerator*, M.S. Thesis, Department of Electrical and Computer Engineering, Michigan State University, East Lansing, Michigan (2004).